Redox-active N4Py-metal complexes in human cell cultures

Geersing, Arjan

Chapter 3

Biological Activity of N4Py-fluorophore Conjugates

Conjugation of different types of molecular fluorophores to the ligand N4Py turned out to have major consequences for the behavior of the conjugates in living cells. Interesting differences in cellular influx as well as the cellular localization were found, which had a large impact on their cytotoxicity towards cancer cells.

A. Geersing
M. G. P. van der Wijst
M. G. Rots
G. Roelfes

3.1 Introduction

The bleomycins (BLMs) are a large family of glycopeptide-derived antitumor antibiotics that were first isolated from *Steptomyces verticillus*.[1,2] They are clinically used in the treatment of various cancers and their antitumor activity is believed to result from their ability to oxidatively cleave 5'-GC-3' and 5'-GT-3' sequences in DNA selectively.[3–7] Various models for the metal binding site of BLM have been reported that have been used to broaden the understanding of its DNA oxidation mechanism,[8–20] and many of them proved to be efficient compounds for oxidative cleavage of plasmid DNA.[9,12,16,19–22] Interestingly, only very few of them have been reported to be effective in cultured cells.[23–25] In addition to BLM mimics, other complexes based on Cu(II),[26–37] Zn(II)[38–40] and Fe(II)[23–25] that were able to cleave DNA have also been reported. Even though some biological studies have been performed to understand the biological cell signaling pathways that are involved in the cellular working for some of these complexes, little attention has generally been given to their cellular localization and proper localization studies by means of fluorescence microscopy have generally not been reported. However, understanding the cellular localization of a compound is important to understand its biology in the cell and *vice versa*.[41,42]

Previous reports by our group have shown that the Fe(II) complex of the pentadentate ligand N,N-bis(2-pyridylmethyl)-N-bis(2-pyridyl)-methylamine (N4Py), is an excellent structural[43–48] and functional[49–52] mimic of Fe(II)-BLM. More recently, the cellular responses to treatment with N4Py-based reagents have been compared to those of BLM.[53] Interestingly, the cellular behavior for Fe(II)-N4Py differs considerably from BLM: whereas BLM induces cell cycle arrest, that ultimately results in mitotic catastrophe,[54] Fe(II)-N4Py was shown to be cytotoxic to cells and the observed double strand breaks were believed to be caused partially by the induction of apoptosis as well as indirect effects such as oxidative damage to other cellular components. Nevertheless, Fe(II)-N4Py was shown to induce nuclear DNA cleavage in living cells as efficiently as BLM.

Knowing the intracellular localization of N4Py will be essential to understand the biology behind the intracellular effects. This knowledge, together with previous mechanistic studies on N4Py and its ease of synthesis, may ultimately result in N4Py, or possibly an N4Py derivative, becoming an interesting anti-cancer agent. In order to gain more insight into the localization of N4Py in cancer cells, we synthesized N4Py-fluorophore conjugates based on Rhodamine B, Cy5 and Fluorescein. The

work described in here will demonstrate that conjugation of a fluorophore to the ligand N4Py can have tremendous effects on the intracellular localization, the biological activity, as well as its mode of transport into the cell. In addition, this work illustrates that great care should be taken in extrapolating conclusions from data obtained with fluorescent conjugates to the parent compounds.

3.2 Results

3.2.1 Synthesis and Spectroscopic Properties of N4Py-fluorophores

Our design for conjugation of N4Py to the fluorophores relies on functionalization of one of its pyridine rings with an amino linker via amide bond formation, to form N4Py-propylamine (Scheme S1). The selected fluorophore derivatives of Rhodamine B (**1**), Cyanine 5 (Cy5, **2**), Fluorescein (**3a**) and (a less polar) methylated version of fluorescein (**3b**), were conjugated to N4Py-propylamine using carbodiimide amide bond formation chemistry (Scheme 1, Schemes S2-4). The products were analyzed by LC-MS as well as ^{1}H-NMR, which showed clear changes in chemical shifts for the signals of the methine singlet and the two pairs of methylene singlets of the N4Py moiety after conjugation to the fluorophores. The compounds were subsequently purified by preparative reversed-phase HPLC and their identities were confirmed by High Resolution Mass Spectrometry (HRMS).

The N4Py-fluorophore conjugates were evaluated under simulated physiological conditions (PBS buffer, pH 7.4). UV/Vis absorption spectroscopy showed a marked bathochromic shift of the absorption bands in the visible region for all N4Py-conjugates compared to their parent fluorophores (Table S1, Figure S1). In addition, all N4Py-conjugates show a diminished molar absorptivity at λ_{max} (Table S1), which is most substantial for N4Py-Fluorescein ($68.8 \cdot 10^3 \pm 0.4 \cdot 10^3$ M^{-1} cm^{-1} to $38.6 \cdot 10^3 \pm 1.4 \cdot 10^3$ M^{-1} cm^{-1}). The general shapes of the fluorophore charge transfer bands remained the same for all compounds, except N4Py-Fluorescein-Me. This result is clearly a consequence of methylation of the phenolic alcohol which effectively changes the total charge of the molecule from anionic to neutral, which causes the shape of the spectrum to change.[55,56] This also explains the much lower molar absorptivity and hypsochromic peak shifts compared to Fluorescein at pH 7.4.

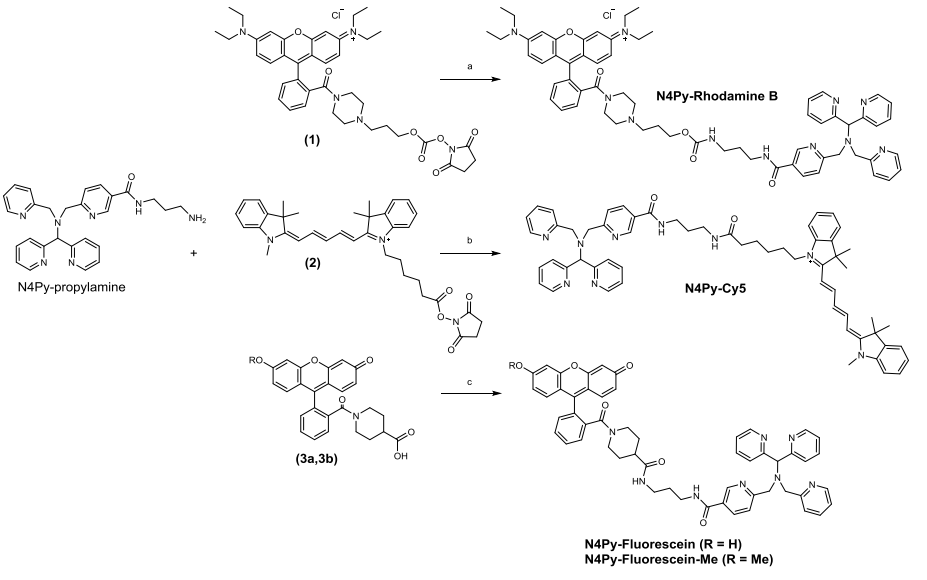

Scheme 1. Synthesis of N4Py-fluorophore conjugates. Reagents and conditions: (a) N4Py-Rhodamine B (N4Py-Rhodamine B) – pyridine, RT, o/n; (b) N4Py-Cyanine 5 (N4Py-Cy5) – *N,N'*-diisopropylcarbodiimide (DIC), OxymaPure, DIPEA, DMF, rt, 20 h; (c) N4Py-Fluorescein (R = H) and N4Py-methyl-Fluorescein (N4Py-Fluorescein-Me; R = Me) – DIC, OxymaPure, DIPEA, DMF, rt, 20 h.

Emission spectra of the N4Py-conjugates showed similar emission bands compared to the parent fluorophores (Figure S2). The conjugates do however display smaller Stokes shifts compared to the parent dyes, with the exception of N4Py-Fluorescein-Me (Table S1). Since cell studies require relatively long incubation times (at least 24 h), the N4Py-conjugates were tested for their photostability over a period of 3 days and the photofading was compared to the parent fluorophores (Figure S3). Under typical physiological conditions (aerated PBS, pH 7.4, ambient light) the conjugates typically showed a limited decrease in emission intensities of roughly 5 %, which is similar to the decrease observed for the parent dyes (Figure S3). In order to test the photostability to irradiation, the conjugates were irradiated for 1 h at their excitation wavelengths and their decrease in emission was followed in time (Figure S4). The N4Py-conjugates were at least as stable under the indicated conditions as the parent fluorophores. The limited degree of photofading of the N4Py-conjugates over time and during irradiation therefore makes them suitable for practical applications.

3.2.2 DNA Cleavage

The iron(II)-complexes of the N4Py-conjugates were generated *in situ* by

complexation to $(NH_4)_2Fe(II)(SO_4)_2 \cdot 6H_2O$ prior to use and the DNA cleavage activities of these N4Py-complexes were subsequently studied using supercoiled pUC18 plasmid at 37°C, pH 8.0. The experiments were carried out in the presence of 1 mM dithiothreitol (DTT) as a reductant to increase the rate of DNA cleavage. The final concentration of the complexes corresponds to 1 µM, with a stoichiometry of 1:150 with regard to DNA base pairs. DNA cleavage activities for the Fe(II)-N4Py-conjugates were determined within 60 min (Figure S5). This data clearly shows that, under these conditions, extensive DNA cleavage was observed for all N4Py-conjugates.

The number of single- and double-strand cuts per DNA molecule were determined for each compound using statistical analysis and plotted as the number of double-strand breaks (*m*) against the number of single-strand breaks (*n*) (Figure S6). Evidently, all compounds seem to follow the Freifelder-Trumbo relationship quite well, which describes a purely single-strand cleavage pathway.[57] Double-strand breaks are therefore not caused directly, but are instead the result of extensive nicking of supercoiled DNA. This is in full agreement with the behavior of the parent complex (Fe(II)-N4Py).[49]

The average amount of single-strand cuts per DNA molecule can be calculated and plotted against time for all Fe(II)-N4Py-conjugates (Figure 1a). The pseudo-first-order rate constants (k_{obs}) were obtained from the linear fit of these plots. The apparent pseudo-first-order rate constants (k^*), taking into account the concentrations of DNA and iron complex, were subsequently used to describe the DNA cleavage efficiency of the Fe(II) complexes and their turnover frequencies (TOF) are presented in Figure 1b. Small differences in TOF were observed, with a slightly higher value for N4Py-Rhodamine B and slightly lower values for all other N4Py-conjugates compared to Fe(II)-N4Py.

The combined results indicate that the intrinsic oxidation chemistry of the N4Py moiety is retained in all conjugates, with DNA cleavage rates that are within close range of Fe(II)-N4Py and a cleavage mechanism that is clearly that of a single strand cutting agent for all investigated compounds. The differences in DNA cleavage efficiency are small and likely the result of differences in noncovalent interactions of the Fe(II)-N4Py-conjugates with DNA.

a)

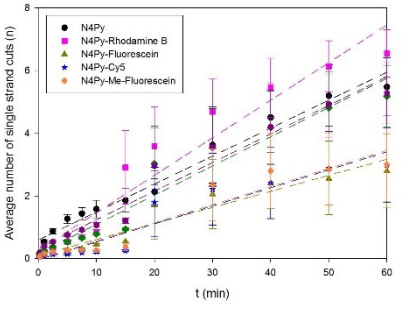

b)

Complex:	TOF (s^{-1})
Fe(II)-N4Py	0.33 (± 0.010)
Fe(II)-N4Py-Rhodamine B	0.44 (± 0.013)
Fe(II)-N4Py-Fluorescein	0.19 (± 0.006)
Fe(II)-N4Py-Fluorescein-Me	0.21 (± 0.006)
Fe(II)-N4Py-Cy5	0.21 (± 0.006)

Figure 1. Quantification of single-strand cuts per DNA molecule induced by iron complexes of N4Py-conjugates. (**a**) Number of single-strand cuts per DNA molecule (*n*) as a function of time. Conditions: Tris-HCl buffer (pH 8.0) at 37°C, 1.0 µM complex, 0.1 µg/µL pUC18 plasmid DNA (150 µM in base pairs), 1.0 mM DTT. Error bars represent the uncertainty limits of *n* and *m*, based on Monte-Carlo simulations, taking into account a standard deviation σ of 0.03 for each individual data point. (**b**) Turnover frequencies (TOF, turnover number per second) of single strand cuts in presence of DTT for Fe(II)-N4Py, Fe(II)-N4Py-Rhodamine B, Fe(II)-N4Py-Fluorescein, Fe(II)-N4Py-Fluorescein-Me and Fe(II)-N4Py-Cy5.

3.2.3 Cell Studies

Since the above results show that the inherent DNA cutting activity of the N4Py moiety did not change significantly upon conjugation of the different fluorophores, the cellular response toward all N4Py-conjugates was determined in SKOV3 ovarian cancer cells using an MTS assay. The MTS assay measures the metabolic activity and, as such, provides a rough indication of putative cytotoxic or cytostatic effects. It is expected that the N4Py-conjugates are able to coordinate iron in the cells, as explained for N4Py in chapter 2. As shown in Figure 2, N4Py-Cy5 shows comparable behavior to Fe(II)-N4Py. In contrast, N4Py-Rhodamine B shows only about one-third of the activity of Fe(II)-N4Py, whereas conjugation to Fluorescein or methyl-Fluorescein results in a complete loss of activity in living cells.

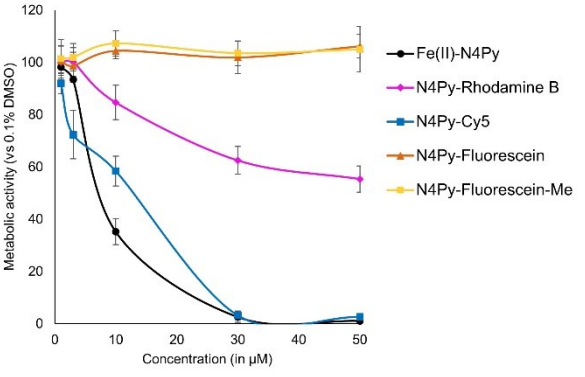

Figure 2. Metabolic activity upon treatment with N4Py-conjugates (MTS assay). Metabolic activity of SKOV3 cells treated for 24 h with 1, 3, 10, 30, 50 µM of Fe(II)-N4Py, N4Py-Rhodamine B, N4Py-Cy5, N4Py-Fluorescein and N4Py-Me-Fluorescein. For each experiment, every treatment was performed in triplicate and the experiment was carried out in triplo. Data are presented as the mean ±SEM.

To determine whether the effect on metabolic activity can be explained by a cytotoxic effect, SKOV3 cells were treated with 10 µM (only N4Py-Cy5 and Fe(II)-N4Py) and 30 µM of the N4Py-conjugates. Subsequently, the percentage of late apoptotic/necrotic cells was determined using a propidium iodide (PI)/FACS assay (Figure 3).[53,58–60] In line with the MTS assay, N4Py-Fluorescein and N4Py-Fluorescein-Me were found not to induce any cell death. Interestingly, N4Py-Rhodamine B did not induce any cell death either. This points to a possible cytostatic effect of N4Py-Rhodamine B. On the other hand, N4Py-Cy5 induced similar (at 10 µM) or even increased (at 30 µM) levels of cell death compared to Fe(II)-N4Py.

To reveal whether the observed cell death was a result of apoptosis, cells were co-treated with the N4Py-conjugates and the pan-caspase inhibitor zVAD-FMK.[61] Strikingly, in contrast to Fe(II)-N4Py,[50] the cell death induced by N4Py-Cy5 could not be inhibited by zVAD-FMK (Figure 3). This suggests that the mechanism of cell death induced by N4Py-Cy5 is caspase-independent.

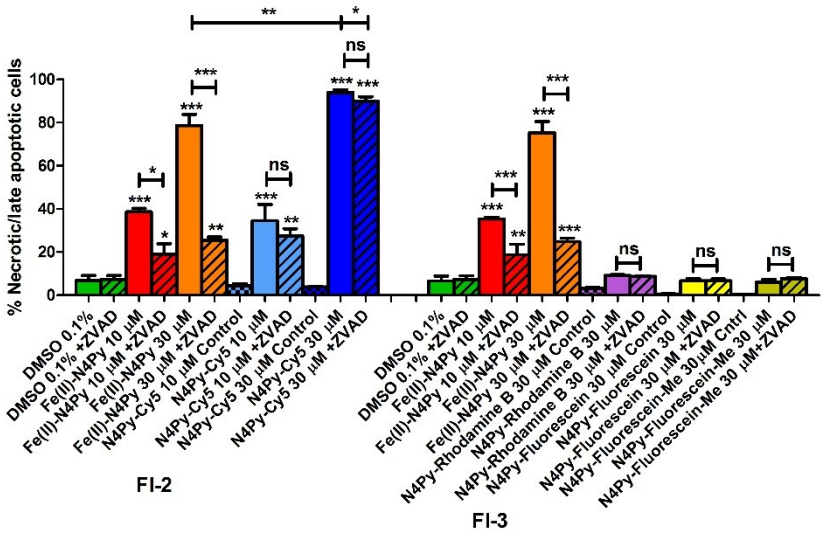

Figure 3. Percentage of necrotic/late apoptotic cells upon treatment with N4Py-conjugates. FACS analysis of propidium iodide (PI) as a marker for necrotic/late apoptotic cells was used to determine the level of cell death upon a 24h treatment of SKOV3 cells with 10 µM and 30 µM of N4Py-conjugates. To determine the contribution of caspase-dependent apoptosis to the total cell death, cells were treated in the presence or absence of the apoptosis-inhibitor zVAD-FMK (20 µM). To prevent fluorescent interference between the N4Py-conjugates and PI signal, PI was either measured in the FL2 (left graph) or FL3 (right graph) channel. PI non-treated cells were used as background control for each separate N4Py-conjugate. As a positive control, Fe(II)-N4Py was measured in both channels. Data are presented as the mean ± SEM from three independent experiments. *** $P < 0.001$; ** $P < 0.01$; * $P < 0.05$; ns, not significant.

Since the inherent DNA cleavage activity of Fe(II)-N4Py compounds can be explained by their ability to generate highly reactive oxygen species (hROS),[43–48,62] it was determined whether this ability remained active in living cells. hROS production in cells treated with the N4Py-conjugates was measured using the APF ROS probe.[63] N4Py-Fluorescein treated cells could not be measured, due to spectral overlap with APF fluorescence. As shown in Figure 4, all measured N4Py-conjugates retained their ability to produce hROS. However, hROS production was less efficient for N4Py-Rhodamine B compared to Fe(II)-N4Py treated cells, even at a three times higher concentration of N4Py-Rhodamine B compared to Fe(II)-N4Py. Detection of hROS via APF probe clearly shows an increase in mean fluorescent intensity (MFI) for Fe-N4Py, N4Py-Cy5 and N4Py-Rhodamine B compared to DMSO control, suggesting that the mechanism of action is oxidative for the N4Py-conjugates and therefore comparable to that of Fe(II)-N4Py.[50]

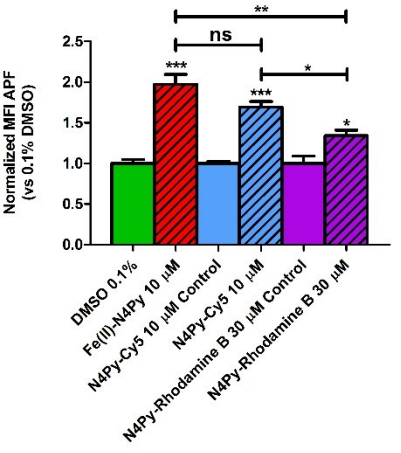

Figure 4. hROS production upon treatment with N4Py-conjugates. The normalized APF ROS probe mean fluorescence intensity (MFI) was measured upon treatment of SKOV3 cells with the N4Py-conjugates. To determine possible interference between the fluorophores and APF fluorescence, each of the N4Py-fluorophore treated cells were measured without the addition of APF (control conditions). Each bar shows the mean ± SEM of three independent experiments. *p < 0.05; **p < 0.01; ***p < 0.001; ns, not significant.

Since the N4Py-conjugates clearly showed oxidative DNA cleavage activity on 'naked' DNA (Figures 1 and S7), and they conserved their ability to induce hROS in living cells (Figure 4), it was investigated whether the ability to induce nuclear DNA damage remained as well. As marker for dsDNA breaks, phosphorylation of serine 139 of histone 2 AX (γH2AX) was used. To minimize the contribution of apoptosis in dsDNA cleavage, flow cytometric analysis of γH2AX was combined with PI (Figure 5). In contrast to figure 3, we used PI here to determine the total cellular DNA content, as this reflects the cell cycle phase of the cells.[58,59] The cells that harbor less DNA than cells in the G1 phase of the cell cycle (the subG1 peak), reflect the (late) apoptotic cell population. These cells were removed from the analysis in order to gain a better estimation of the direct DNA damage induced by the N4Py-conjugates.[50] The N4Py-Fluoresceins were excluded from this analysis, as neither metabolic activity nor cell death were affected by these compounds.

As observed in Figure 5, both N4Py-Rhodamine B and N4Py-Cy5 showed an increase in the number of dsDNA breaks compared to solvent control. However, a clear difference in the number of γH2AX positive cells was observed: treatment with N4Py-Rhodamine B showed only a small amount of γH2AX positive cells (12.6% ±

1.2) compared to Fe(II)-N4Py (32.0 % ± 3.3 FI-2; 27.4 % ± 4.1), whereas a much higher value for N4Py-Cy5 treated cells was found (51.1 % ± 3.0).

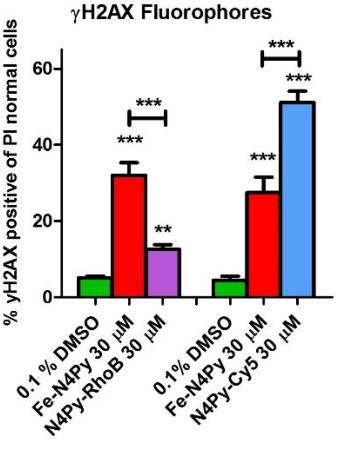

Figure 5. dsDNA damage in non/early apoptotic cells upon treatment with N4Py-conjugates. SKOV3 cells were treated for 24 h with 30 μM N4Py-Rhodamine B and N4Py-Cy5. dsDNA damage was assessed by γH2AX-Alexa 647 (for N4Py-Rhodamine B) or γH2AX-Alexa 488 (for N4Py-Cy5). To minimize the contribution of apoptosis-induced dsDNA damage, apoptotic cells (in the subG1 peak), stained by PI, were excluded from the analysis. The gate for γH2AX positive cells in solvent control was set at 5 %. Each value represents mean ± SEM from three independent experiments.

All cell culture experiments performed so far, clearly indicate a different behavior of the different N4Py-fluorophores (Figures 2-5), despite showing comparable inherent properties for oxidative DNA cleavage under cell-free conditions (Figures 1, S7 and S8). To explain this observation, the cellular localization of the N4Py-conjugates was determined using confocal microscopy. The absence of cellular activity of N4Py-Fluorescein could be explained by its inability to enter the cell (Figure S7a). Furthermore, the influx properties of N4Py-Fluorescein could not be completely attributed to its negative charge, as methylation of the alcohol group did not improve cellular influx (Figures S7b,c).[64]

Both N4Py-Rhodamine B and N4Py-Cy5 could enter the cell (Figures S7d,e). To reveal their cellular localization, cells treated with both N4Py-fluorophores were co-stained with Mitotracker and Lysotracker, staining the mitochondria and lysosomes, respectively. These studies showed that the cellular distribution between N4Py-Rhodamine B and N4Py-Cy5 was very different; 24h treatment with N4Py-Rhodamine B showed a predominant lysosomal localization (Figure 6b), whereas

N4Py-Cy5 preferentially localized to the mitochondria (Figure 7a). Notably, over time, the localization of N4Py-Cy5 toward the lysosomes increased (Figures 7b, 7d and 8). In case of N4Py-Rhodamine B, the localization of the N4Py-conjugate (Figures 6a and 6b) differed from the parental Rhodamine B fluorophore (Figures 6c and 6d), whereas the parental Cy5 fluorophore behaved similarly as the N4Py conjugate.

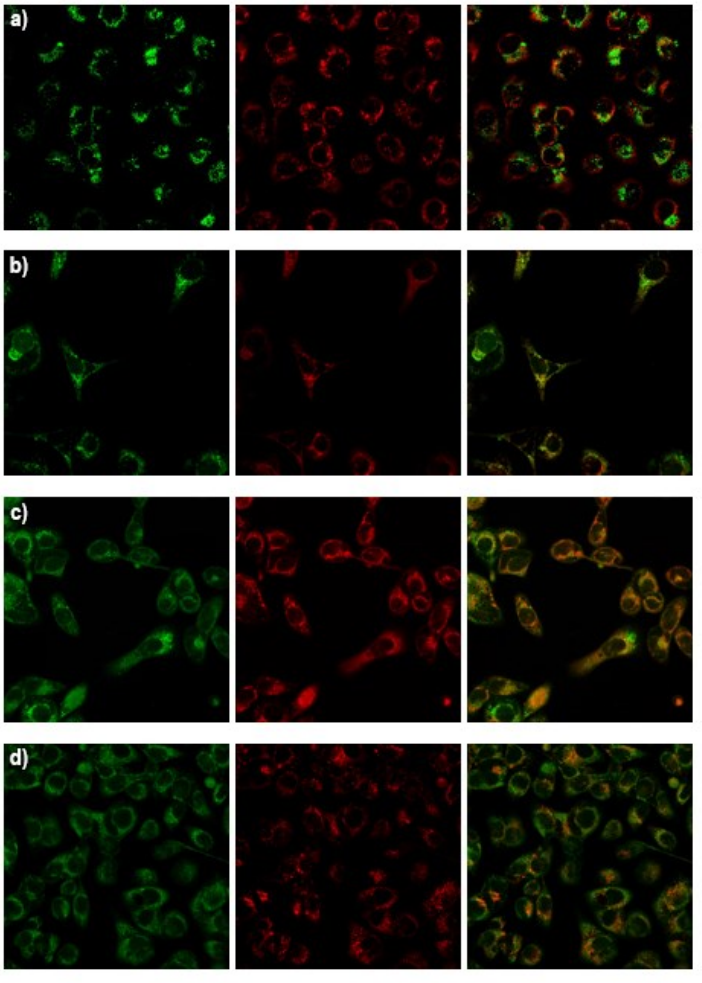

Figure 6. Localization of N4Py-Rhodamine B and Rhodamine B. Confocal microscopy images of N4Py-Rhodamine B and Rhodamine B, with (from left to right): (**a**) N4Py-Rhodamine B, Mitotracker Deep Red, channel overlay, 24h treatment; (**b**) N4Py-Rhodamine B, Lysotracker Deep Red, channel overlay, 24h treatment; (**c**) Rhodamine B, Mitotracker Deep Red, channel overlay, 1h treatment; (**d**) Rhodamine B, Lysotracker Deep Red, channel overlay, 1h treatment.

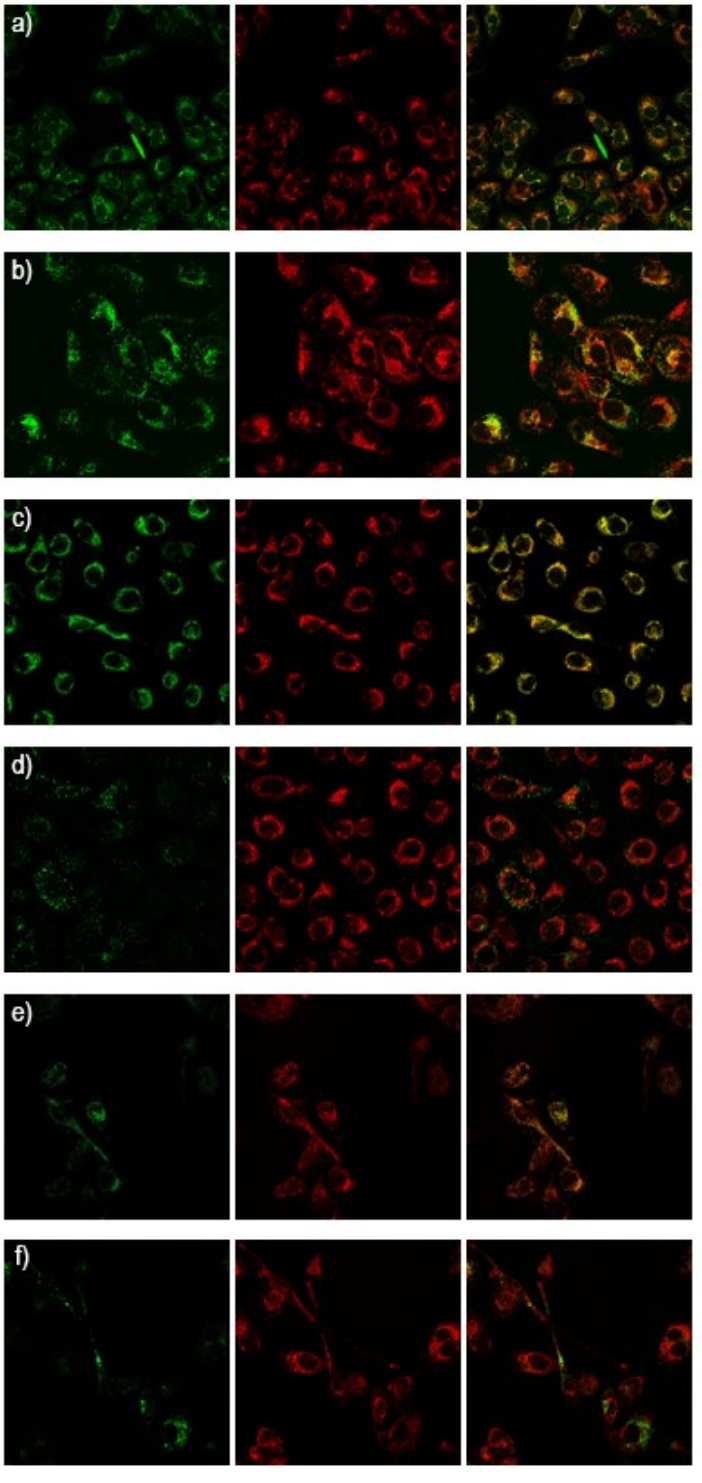
a)
b)
c)
d)
e)
f)

Figure 7. (previous page) Localization of N4Py-Cy5 and Cy5-COOH. Confocal microscopy images of N4Py-Cy5 and Cy5-COOH, with (from left to right): (**a**) N4Py-Cy5, Mitotracker Green, channel overlay, 24h treatment; (**b**) N4Py-Cy5, Lysotracker Green, channel overlay, 24h treatment; (**c**) N4Py-Cy5, Mitotracker Green, channel overlay, 1h treatment; (**d**) N4Py-Cy5, Lysotracker Green, channel overlay, 1h treatment; (**e**) Cy5-COOH, Mitotracker Green, channel overlay, 1h treatment; (**f**) Cy5-COOH, Lysotracker Green, channel overlay, 1h treatment.

Quantification of colocalization was performed using Pearson's Correlation Coefficient (PCC) (Figure 8).[65] As a positive control for co-localization, cells were co-stained with Mitotracker Green and Deep Red, whereas a 90 degree rotation of the Mitotracker Green image was used as a negative control (Figure 8). 1 h treatment of cells with N4Py-Cy5 showed very similar behavior compared to the parent Cy5-COOH fluorophore, with high localization in the mitochondria (PCC = 0.86 vs 0.73) and low localization in the lysosomes (PCC = 0.14 vs 0.20). Longer exposure of cells to N4Py-Cy5 (1h vs 24h treatment) significantly increased lysosomal localization (PCC = 0.14 vs 0.58) while slightly decreasing mitochondrial presence (PCC = 0.86 vs 0.75). Contrary to N4Py-Cy5, 1 h treatment with N4Py-Rhodamine B did not show any detectable uptake in the cells, suggesting slow uptake (*vide infra*, Figure 8). 24 h treatment with N4Py-Rhodamine B revealed mainly lysosomal localization with little presence in the mitochondria (PCC = 0.71 vs 0.23), a result contrary to the parent Rhodamine B fluorophore (PCC = 0.46 vs 0.77).

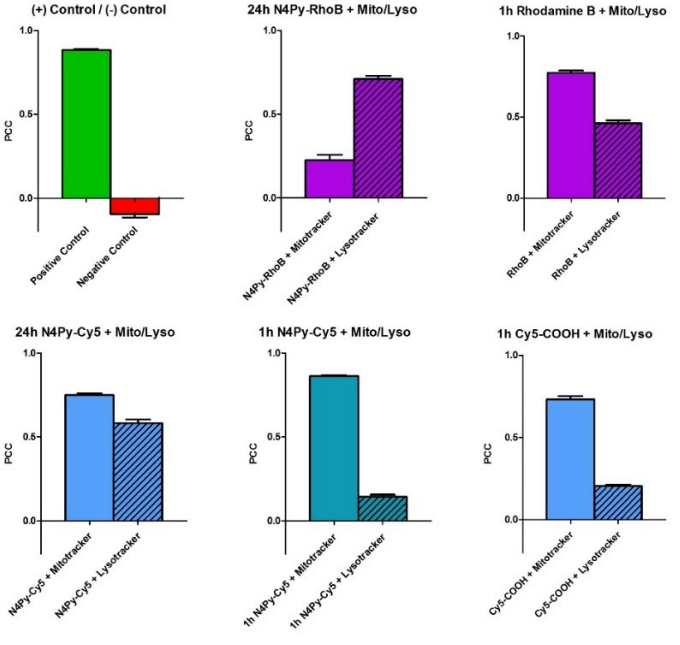

Figure 8. (previous page) Pearson Correlation Coefficients (PCC) for colocalization studies of N4Py-conjugates and parent fluorophores. SKOV3 cells were treated for the indicated times with the N4Py-conjugates or their parent fluorophores. For each treatment, the level of colocalization with either the Mitotracker or Lysotracker dye was calculated using PCCs. The positive control represents the colocalization of Mitotracker Green and Deep Red, whereas the negative control represents a 90 degree rotation of the Mitotracker Green image. Each bar shows the mean ± SEM.

The differences in localization between the parental fluorophores and the N4Py-conjugates, and between both N4Py-conjugates, may be explained by their mode of transport into the cell. To determine whether the mode of transport is active or passive, SKOV3 cells were treated for 24h with N4Py-Rhodamine B and N4Py-Cy5 at different temperatures. In contrast to passive transport, active transport decreases tremendously with decreased temperature, and is completely shut down at 4 °C.[66–68] The effect of temperature on active versus passive transport is clearly shown in Figure 9; the cellular influx of N4Py-Rhodamine B is completely shut down at 4°C, and decreased at 25.8°C, whereas the cellular influx of N4Py-Cy5 seems hardly affected by temperature. This suggests an active mode of transport for N4Py-Rhodamine B and a passive mode of transport for N4Py-Cy5. The transport mechanism of N4Py-Cy5 therefore seems to be similar to that of the parent N4Py ligand and Fe(II)-N4Py complex (Figure S8).

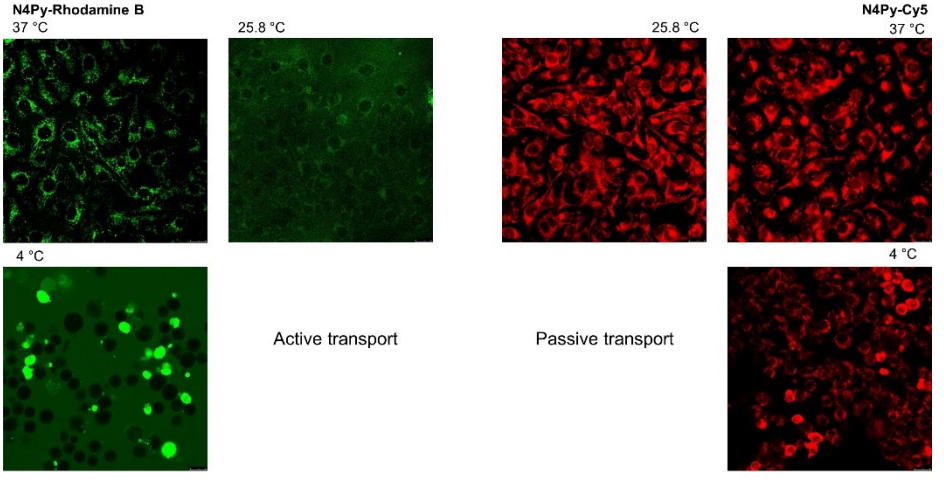

Figure 9. The effect of temperature (T = 37°C, 25.8°C and 4°C) on the localization of N4Py-Rhodamine B and N4Py-Cy5.

Since N4Py-Cy5 predominantly accumulates in the mitochondria (Figures 7 and 8) and generates hROS (Figure 4), it may damage the mitochondria and its DNA.[69] Indeed, qPCR revealed that 40 ± 7.7 % of the mtDNA was degraded in the cells threated with N4Py-Cy5, but not with the other N4Py conjugates or Cy5-COOH (Figure 10). As a result of all this, the damaged mitochondria can become dysfunctional, and this could lead to electron leakage from the electron transport chain and the generation of mitochondrial superoxide.[70] The mitochondrial superoxide production was therefore determined with the fluorescent probe MitoSOX.[71–73] As shown in Figure 11, mitochondrial superoxide production was increased specifically in cells treated with N4Py-Cy5 and not with the other N4Py-conjugates. However, this finding seems to be only partly dependent on N4Py, since Cy5-COOH itself already induced mitochondrial superoxide production, albeit at slightly lower levels than N4Py-Cy5. Nevertheless, when taken into account the reduced number of mitochondria (Figure 10), the mitochondrial superoxide production per mitochondrion did increase at least two-fold more in the N4Py-Cy5 treated compared to the Cy5-COOH treated cells.

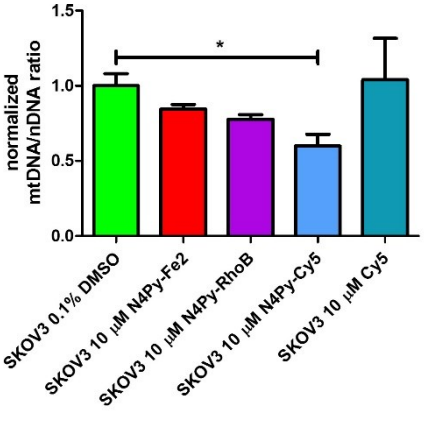

Figure 10. Mitochondrial DNA copy number upon treatment with N4Py-fluorophores. The normalized mitochondrial DNA copy number was determined upon treatment of SKOV3 cells with Fe(II)-N4Py, N4Py-Rhodamine B, N4Py-Cy5 and Cy5-COOH. Each bar represents the mean ± SEM of at least three independent experiments. *$p < 0.05$.

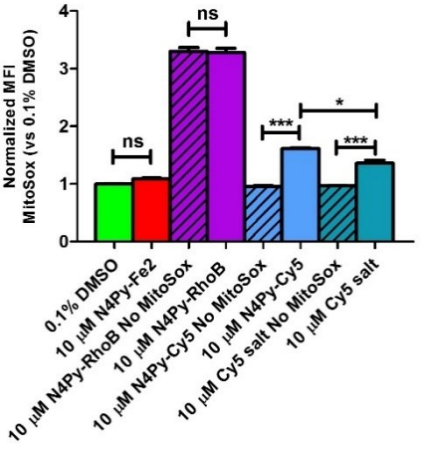

Figure 11. Mitochondrial superoxide production upon treatment with N4Py-conjugates. The normalized MitoSox Red mean fluorescent intensity (MFI) was determined upon treatment of SKOV3 cells with Fe(II)-N4Py, N4Py-Rhodamine B, N4Py-Cy5 and Cy5-COOH. To determine possible interference between the fluorophores and MitoSox Red fluorescence, N4Py-fluorophore treated cells were measured without the addition of MitoSox Red. Data values are mean ± SEM of three independent experiments. *$p < 0.05$; **$p < 0.01$; ***$p < 0.001$; ns, not significant.

Mitochondrial dysfunction is detrimental for cells and is linked to a wide variety of diseases and aging.[74] Therefore, proper removal of dysfunctional mitochondria is essential for cell survival. Cells can do this by non-selective autophagy ("self-eating") and by mitophagy, a mitochondria-specific type of autophagy.[75] Such a survival mechanism has been described for cells exposed to various stressors, including oxidative stress.[76] However, in our study, no evidence for mitophagy has been found upon treatment with N4Py-Cy5; co-localization studies in 0.1% DMSO control versus N4Py-Cy5 treated cells using Mitotracker Green and Lysobrite Red stainings[77] revealed that there is no increase in co-localization between the mitochondria (Mitotracker Green) and the lysosomes (Lysobrite Red) upon treatment with N4Py-Cy5 (Figure 12).

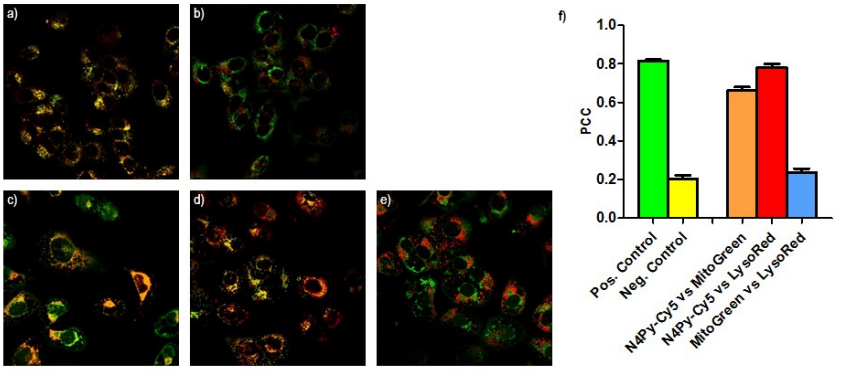

Figure 12. Co-localization studies with N4Py-Cy5, Mitotracker Green and Lysobrite Red. Confocal images of SKOV3 cells treated for 24h with 0.1% DMSO (a, b) or 10 µM N4Py-Cy5 (c, d, e): (a) Lysobrite Red with Lysotracker Deep Red (positive control); (b) Mitotracker Green with Lysobrite Red (negative control); (c) N4Py-Cy5 with Mitotracker Green; (d) N4Py-Cy5 with Lysobrite Red; (e) Mitotracker Green with Lysobrite Red; (f) Pearson correlation coefficient (PCC) for all co-localization experiments (a-e).

3.3 Discussion

In this study, we described the effect of fluorescent-labeling on the mode of transport, cellular localization and biological activity of the BLM-mimic N4Py. Even though conjugation of fluorophores had only a slight effect on the intrinsic DNA cleavage activity of the N4Py moiety, its intracellular behavior was greatly affected. This is attributed to a change in mode of transport and localization of the N4Py molecule upon conjugation with the different fluorophores: N4Py-Fluorescein was unable to pass through the cell membrane, resulting in a lack of cellular activity. In contrast, N4Py-Rhodamine B and N4Py-Cy5 could both enter the cell, but localized to different compartments.

Whereas N4Py-Cy5 passively entered the cell and predominantly localized in the mitochondria, N4Py-Rhodamine B was actively transported into the cell and remained trapped in the lysosomes. As a result, N4Py-Rhodamine B remained largely inactive in the cell. In addition, the mitochondrial localization of N4Py-Cy5 seemed to improve the cytotoxicity of the molecule in comparison to N4Py. Interestingly, the mitochondrial localization also changed the mode of cell death compared to the parental molecule.

In line with previous observations, Fe(II)-N4Py predominantly induced caspase-dependent apoptosis,[53] whereas the cell death induced by N4Py-Cy5 was caspase-

independent. Since N4Py-Cy5 did not localize to the nucleus, we can exclude the direct induction of dsDNA breaks (γH2AX positive cells) by N4Py-Cy5 itself. Alternatively, dsDNA breaks can be induced indirectly via programmed cell death. As caspase-dependent programmed cell death (apoptosis) did not take place upon treatment with N4Py-Cy5, it is proposed that caspase-independent cell death indirectly induced the increase in γH2AX. In addition to apoptosis (caspase-dependent, γH2AX positive) and necrosis (caspase-independent, γH2AX negative), many other forms of cell death exist that may explain the N4Py-Cy5 induced cell death (caspase-independent, γH2AX positive).[78]

One such mode of cell death that may explain the N4Py-Cy5 induced cell death is programmed necrosis, more specifically parthanatos.[79] This form of cell death induces the sequential activation of poly ADP ribose polymerase-1, calpains, Bax, and eventually the translocation of apoptosis-inducing factor from the mitochondria to the nucleus.[80] This event will, via the phosphorylation of γH2AX, contribute to chromatinolysis and cell death.[81] This type of cell death can be induced by a variety of stressors, including DNA alkylating agents[81] and ROS-induced mitochondrial dysfunction.[82] Since treatment with N4Py-Cy5 induced mitochondrial dysfunction (increased mtROS production, decreased mtDNA copy number), parthanatos could be a plausible mode of cell death induced by N4Py-Cy5.

Many tumors are or will become resistant to apoptosis during therapy, for example, by overexpressing anti-apoptotic or suppressing pro-apoptotic proteins.[83] Therefore, induction of cell death via an alternative route, as was shown for N4Py-Cy5, may be a promising strategy to induce cell death in apoptosis-resistant tumors. SKOV3 cells have been shown to exhibit some resistance to apoptosis,[84] and therefore, N4Py-Cy5 may improve the cytotoxicity of the parental molecule. Indeed, our data shows increased induction of cell death and dsDNA breaks upon treatment with N4Py-Cy5 compared to the parental molecule.

The high polarity of Fluorescein is known to often result in low cell permeability, which is especially attributed to the dianionic charge state at physiological pH.[55,85,86] As such, the inability of N4Py-Fluorescein to enter the cell was not completely unexpected. The absence of cellular influx can explain the fact that metabolic activity was unaltered upon treatment with this compound. Moreover, the unaltered metabolic activity strongly suggests that lipid/membrane oxidation by N4Py is not a major contributor to its cellular cytotoxicity.

Improved cell permeability can be obtained by protection of Fluorescein as its diester.[87] However, this chemical modification requires intracellular esterases to unmask the fluorophore and, most importantly, the acetyl ester moieties are reportedly unstable.[88] For that reason, N4Py-Fluorescein-Me was synthesized as an alternative, which contains a stable methoxy group instead of an unstable acetate functionality. Methylated Fluorescein is reported to be eight times more stable than Fluorescein with much less variable emission due to pH changes and is expected to be less polar compared to Fluorescein.[64] Conjugation to N4Py did however not result in better cellular influx compared to N4Py-Fluorescein. It does, however, provide further evidence that N4Py does have to enter the cell in order to cause cellular damage.

Conjugation of Rhodamine B to N4Py shows mainly localization in the lysosomes without any significant accumulation in the mitochondria, which seems to be explained by the cellular influx: whereas Rhodamine B enters the cell passively and localizes in the mitochondria,[89] N4Py-Rhodamine B enters the cell via active transport, thus making an endocytic membrane trafficking pathway with subsequent delivery of N4Py-Rhodamine B to the lysosomes very likely.[90,91] The difference in the mode of transport might, at least in part, be explained by the change in lipophilicity due to conjugation of Rhodamine B to N4Py.

Analogously, Cy5-COOH was shown to selectively target the mitochondria, suggesting that its structural properties closely resemble that of Rhodamine B. Contrary to N4Py-Rhodamine B, conjugation of Cy5 to N4Py initially shows significant localization in the mitochondria, with an increased localization in the lysosomes over time. This indicates that, initially, the intrinsic properties of Cy5 seem to control the behavior of the entire conjugate with the localization of N4Py-Cy5 likely being membrane-potential driven. However, over time, other factors seem to successfully compete with this membrane-potential driven behavior, as lysosomal localization increased during prolonged incubation times.

A note of caution on the general use of fluorophores in cell studies might be appropriate here, since in addition to changing the behavior of the parent molecule, fluorophores themselves can already affect cellular function.[92] This is displayed by the increase in mitochondrial superoxide production upon treatment of SKOV3 cells with Cy5-COOH, which is presumably caused by photooxidation of Cy5-COOH itself, as has been reported previously.[93–96]

In general, conjugation of a fluorescent group to a small molecule can generally be beneficial for tracking the fluorescent analog during biological assays. However, one should always take into account that the structural differences between the conjugate and the parent compound can result in changes in influx, mechanism of transport and cellular localization of the compounds, which in turn can all contribute to a change in the biological activity of the compound. Assuming that the biological activity of the fluorophore conjugate is largely in line with that of the parent (non-fluorescent) molecule can be inaccurate and therefore, result in false conclusions regarding the parent compound. Even though some studies have shown that the fluorophore conjugate can behave quite similar to the parent compound in terms of catalytic efficiency,[97] chemical activity[98,99] or localization,[100] these examples seem to provide the exceptions rather than the rule. Various studies reported reduced binding affinities,[101,102] reduced chemical activities[103,104] or increased aspecificity[105] by introduction of a fluorophore.

3.4 Conclusions

The data described in this study shows that conjugation of a fluorophore to the ligand N4Py has large effects on the intracellular localization, mode of transport into the cell as well as biological activity. Conjugation of Fluorescein to N4Py showed that lipid oxidation by N4Py is not a major contributor to its cellular cytotoxicity, since the lack of cellular influx resulted in unaltered metabolic activity of the cancer cells upon treatment with N4Py-Fluorescein and N4Py-Fluorescein-Me. Localization of N4Py-Rhodamine B in the lysosomes as a result of active transport through the cell membrane results in reduced biological activity in comparison to N4Py and contrasting localization compared to Rhodamine B. In contrast, localization of N4Py-Cy5 in the mitochondria and passive cellular uptake results in enhanced cytotoxicity and nuclear DNA damage in comparison to N4Py at a concentration of 30 μM, with a change in cell death mechanism and increased lysosomal localization upon increased treatment times.

Our work illustrates that great care should be taken in extrapolating conclusions from data obtained with fluorescent conjugates to the parent compounds of interest. We therefore suggest that, in addition to fluorescent labeling, other techniques should be used in order to confirm a hypothesis about cellular localization of biologically active compounds.

3.5 Experimental Section

3.5.1 Materials and Instrumentation

Reagents for synthesis were used as purchased without further purification unless noted otherwise. Cyanine 5 carboxylic acid (Cy5-COOH) and Cyanine 5 NHS ester (Cy5-NHS) were purchased from Lumiprobe. All solvents were reagent grade and dry solvents were taken from an MBraun solvent purification system (SPS-800) when necessary. Moisture sensitive reactions were performed under a nitrogen atmosphere using oven dried glassware and using standard Schlenk techniques. High purity water from a Millipore Milli Q purification apparatus containing a 0.22 µm filter was used when necessary for synthetic purposes. Reaction temperatures refer to the temperature of the oil bath. Column chromatography was performed on silica gel (Silica-P flash silica gel from Silicycle, size 40-63 µm (230-400 mesh)). TLC was performed on silica gel 60/Kieselguhr F_{254} purchased from Merck. Compounds were visible by the naked eye or were visualized with a UV lamp (254 nm). Melting points were recorded on a Büchi B-545 melting point apparatus. NMR spectra were recorded on a Varian VXR-300, Varian Mercury Plus 400 and Agilent 400-MR at 298K. Chemical shifts in ^{1}H and ^{13}C NMR spectra were internally referenced to solvent signals (^{1}H NMR: $CDCl_3$ at δ = 7.26 ppm, $(CD_3)_2SO$ at δ = 2.50 ppm, CD_3OD at δ = 3.31 ppm, CD_3CN at δ = 1.94 ppm, $(CD_3)_2CO$ at δ = 2.05 ppm; ^{13}C NMR: $CDCl_3$ at δ = 77.16 ppm, $(CD_3)_2SO$ at δ = 39.52 ppm, CD_3OD at δ = 49.00 ppm, CD_3CN at δ = 1.32 ppm, $(CD_3)_2CO$ at δ = 29.84 ppm) Data are reported as follows: chemical shifts (δ), multiplicity (s = singlet, d = doublet, t = triplet, q = quartet, dd = double doublet, m = multiplet, broad = broad band, app. = apparent), coupling constants (*J* (Hz), and integration. High-resolution mass spectrometry was performed on a LTQ Orbitrap XL spectrometer (ESI+, ESI- and APCI). LC-MS analysis were performed on an Acquity H-Class UPLC with Xevo G2 TOF mass detector for HRMS (ESI+) and Acquity UPLC with TQD mass detector for LRMS (ESI+), both manufactured by Waters. All analysis were performed at 35 °C using a reversed-phase UPLC column (Waters Acquity UPLC BEH C8, 130 Å, 1.7 µm, 2.1 mm x 50 mm). UPLC grade water and acetonitrile (CH_3CN) were used as eluents with addition of 0.1% formic acid (FA) to both. The following inlet method was used: (water/ CH_3CN) 95:5 for 5 min, to 40:60 at 12 min, 40:60 for 3 min, to 95:5 in 1 min, at 95:1 for 5 min. Total run time: 21 min. UV absorbance was monitored at 254 nm in combination with the total ion current (TIC). Reversed phase HPLC analysis were performed on a Shimadzu HPLC system equipped with two LC-20AD solvent delivery systems, a DGU-20A3 degasser, a SIL-

20A auto injector, a SPD-M20A diode array detector, a CTO-20A column oven, a CBM-20A system controller and FRC-10A fraction collector. Analysis were performed with a Waters Xterra MS C18 column (3.0 x 150 mm, particle size 3.5 µm) using a gradient of HPLC grade MeOH and double distilled water with addition of 0.1 % TFA to both; gradient A: (MeOH/water) 10:90 for 10 min, to 70:30 at 40 min, 70:30 for 25 min, to 10:90 at 70 min, 10:90 for 10 min (total run time: 80 min); gradient B: (MeOH/water) 10:90 for 10 min, to 70:30 at 25 min, 70:30 for 20 min, to 10:90 at 55 min, 10:90 for 5 min (total run time: 60 min). Flow: 0.5 mL/min at 40°C. Preparative HPLC was performed with a Waters Xterra MS C18 column (7.8 x 150 mm, particle size 10 µm); gradient A or B. Flow: 1 mL/min at 40°C. UV-Vis absorption spectra were recorded at 37°C using a 1 cm path-length quartz cell on a Jasco V-660 spectrophotometer. Absorption maxima are ±2 nm. Molar absorptivities were determined by determination of A_{max} for at least 6 different concentrations in triplicate. Corrected fluorescence emission spectra were recorded at 37°C using a 1 cm path-length quartz cell with a 100 µL (10 x 2 mm) or 1400 µL chamber volume on a Jasco FP-6200, containing a 150W Xenon lamp contained within a sealed housing. Emission maxima are ±3 nm.

3.5.2 Synthesis of N4Py-fluorophore Conjugates and Intermediate Compounds

N4Py[43,47] and N4Py-propylamine[49] (Scheme S1) were synthesized according to established procedures. Rhodamine B[106] and Fluorescein[64] derivatives were synthesized according to literature procedures and all data are in agreement with those reported.

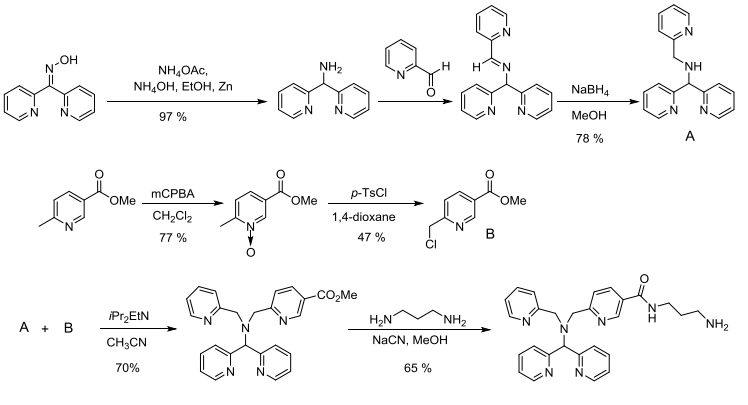

Scheme S1. Synthesis of N4Py-propylamine from di-2-pyridyl ketoxime and methyl 6-methylpyridine-3-carboxylate.

For the synthesis of **N4Py-Rhodamine B**, a procedure from the literature[106] was adapted as follows (Scheme S2): to an oven dried 5 mL round bottom flask under a N_2 atmosphere was added N,N'-disuccinimidyl carbonate (DSC) (64 mg, 0.25 mmol), Rhodamine B-Alcohol (57 mg, 0.10 mmol) and 0.75 mL of dry pyridine. After stirring at room temperature for 4h, additional DSC (38 mg, 0.15 mmol) was added to the flask. After another 3 h, excess DSC was quenched by addition of water (14.8 mg, 0.82 mmol). To this solution, N4Py-propylamine (75 mg, 0.16 mmol) in 0.75 mL dry pyridine was added. The resulting dark purple solution was stirred at room temperature overnight. The solution was subsequently partitioned between 4:1 CH_2Cl_2/^{i}PrOH and water. After isolation of the organic layer, the aqueous layer was extracted 3 more times with 4:1 CH_2Cl_2/^{i}PrOH. The combined organic layers were dried over Na_2SO_4, filtered and concentrated under reduced pressure to yield N4Py-Rhodamine B as a dark purple solid (0.9 mg, 83 %): LC-MS TQD: M^+ calcd 1062.57, found 1062.70 ret. time t = 8.95 min. A high purity sample suitable for cell studies was obtained by preparative HPLC using gradient B. Ret. time: 31.99 min HRMS: M^+ calcd 1062.571, found: 1062.567.

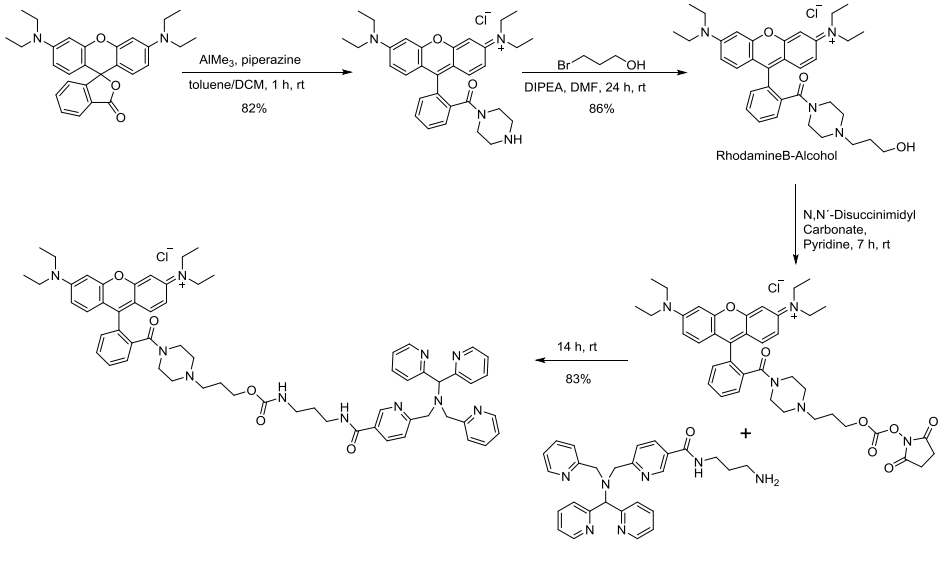

Scheme S2. Synthesis of N4Py-Rhodamine B from Rhodamine B base.

N4Py-Fluorescein (Scheme S3): To an oven dried 10 mL round bottom flask under a N_2 atmosphere was added Fluorescein-COOH (10 mg, 0.023 mmol), N,N′-Diisopropylcarbodiimide (DIC) (7.0 µL, 0.045 mmol),

Ethyl(hydroxyimino)cyanoacetate (OxymaPure) (6.4 mg, 0.045 mmol) and 4 mL of dry N,N-Dimethylformamide (DMF). After stirring at room temperature for 20 min, N4Py-propylamine (11.6 mg, 0.025 mmol) was added to the flask and the deep orange solution was stirred for another 20h at room temperature. The solution was subsequently diluted by addition of DCM (± 25 mL) and washed with sat. $NaHCO_3$ (6 x 25 mL). The organic layer was dried over Na_2SO_4, filtered and concentrated under reduced pressure to yield crude N4Py-Fluorescein as an orange solid: LC-MS TQD: M^+ calcd 893.38, found 893.43 ret. time t = 8.83 min; $[M+Na+K]^+$ calcd 954.32, found 954.37 ret. time t = 8.61 min. A high purity sample suitable for cell studies was obtained by preparative HPLC using gradient B. Ret. time: 31.56 min HRMS: M^+ calcd 893.377, found: 893.377.

N4Py-Fluorescein-Me (Scheme S3): To an oven dried 10 mL round bottom flask under a N_2 atmosphere was added Fluorescein-Me-COOH (10 mg, 0.022 mmol), N,N′-Diisopropylcarbodiimide (DIC) (6.8 µL, 0.044 mmol), Ethyl(hydroxyimino)cyanoacetate (OxymaPure) (6.2 mg, 0.044 mmol), N,N-Diisopropylethylamine (DIPEA) (7.6 µL, 0.044 mmol) and 5 mL of dry N,N-Dimethylformamide (DMF). After stirring at room temperature for 20 min, N4Py-propylamine (13.3 mg, 0.028 mmol) was added to the flask and the deep orange solution was stirred for another 20 h at room temperature. The solution was subsequently diluted by addition of DCM (± 25 mL) and washed with sat. $NaHCO_3$ (6 x 25 mL). The organic layer was dried over Na_2SO_4, filtered and concentrated under reduced pressure to yield crude N4Py-Fluorescein-Me as an orange solid: LC-MS TQD: $[M+H]^+$ calcd 907.39, found 907.38 ret. time t = 9.17 min. A high purity sample suitable for cell studies was obtained by preparative HPLC using gradient B. Ret. time: 24.71 min HRMS: M^+ calcd 907.393, found: 907.392.

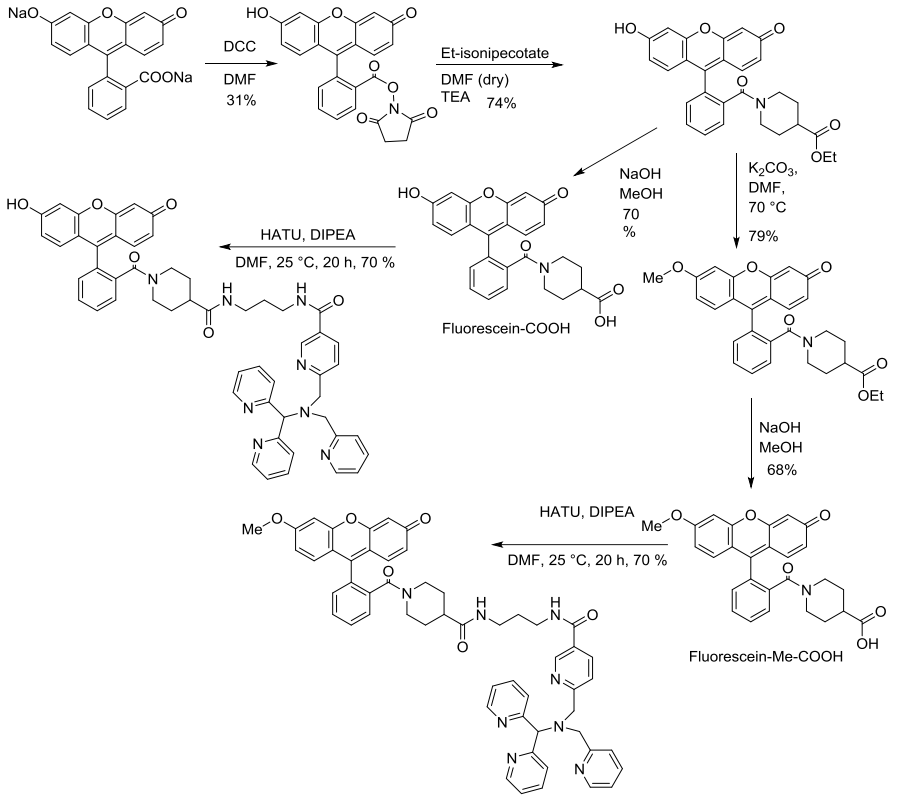

Scheme S3. Synthesis of N4Py-Fluorescein and N4Py-Fluorescein-Me from Fluorescein sodium salt.

N4Py-Cy5 (Scheme S4): To an oven dried 10 mL round bottom flask under a N_2 atmosphere was added Cy5-NHS (10 mg, 0.016 mmol), N,N′-Diisopropylcarbodiimide (DIC) (10.1 µL, 0.065 mmol), Ethyl(hydroxyimino)cyanoacetate (OxymaPure) (9.3 mg, 0.065 mmol), N,N-Diisopropylethylamine (DIPEA) (11.3 µL, 0.065 mmol) and 3 mL of dry N,N-Dimethylformamide (DMF). After stirring at room temperature for 5 min, N4Py-propylamine (9.1 mg, 0.019 mmol) was added to the flask and the deep blue solution was stirred for another 20h at room temperature. The solution was subsequently diluted by addition of DCM (± 25 mL) and washed with sat. $NaHCO_3$ (4 x 25 mL) and sat Na_2CO_3 (2 x 25mL). The organic layer was dried over Na_2SO_4, filtered and concentrated under reduced pressure to yield crude N4Py-Cy5 as a dark blue solid: LC-MS TQD: M^+ calcd 932.53, found 932.58 ret. time t = 10.09 min. A high purity sample suitable for cell studies was obtained by preparative HPLC using gradient B. Ret. time: 28.07 min HRMS: M^+ calcd 932.534, found: 932.534.

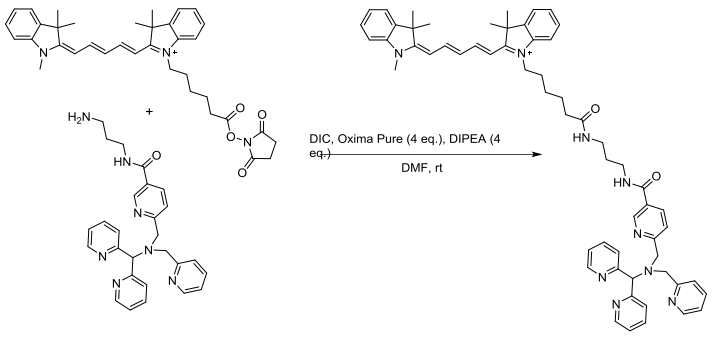

Scheme S4. Synthesis of N4Py-Cy5 from commercially obtained Cyanine 5 NHS ester.

3.5.3 Stability Studies of N4Py-Fluorophore Conjugates

Table S1. Comparison of absorbance λ_{max}, ε_{max}, emission λ_{max} and Stokes shifts between N4Py-conjugates and their parent fluorophores as obtained by UV-Vis absorbance and emission spectra.

	Cy5-COOH	N4Py-Cy5	Fluorescein	N4Py-Fluorescein
λ_{max} (nm)	639	643	491	502
ε_{max} ± SD (M^{-1} cm^{-1})	$12.9 \cdot 10^4$ ($0.30 \cdot 10^4$)	$11.9 \cdot 10^4$ ($0.43 \cdot 10^4$)	$68.8 \cdot 10^3$ ($0.4 \cdot 10^3$)	$38.6 \cdot 10^3$ ($1.4 \cdot 10^3$)
$\lambda_{emission,max}$ (nm)	659	661	515	521
Stokes (cm^{-1})	475	424	949	726

Table S1 continued.

	N4Py-Fluorescein-Me	Rho B	N4Py-Rhodamine B
λ_{max} (nm)	460 (483)	554	568
ε_{max} ±SD (M^{-1} cm^{-1})	$17.0 \cdot 10^3$ ($0.07 \cdot 10^3$) ε_{483} = $15.3 \cdot 10^3$ ($0.08 \cdot 10^3$)	$68.0 \cdot 10^3$ ($0.3 \cdot 10^3$)	$61.5 \cdot 10^3$ ($1.0 \cdot 10^3$)
$\lambda_{emission,max}$ (nm)	522 (549)	587	592
Stokes (cm^{-1})	1547	1015	713

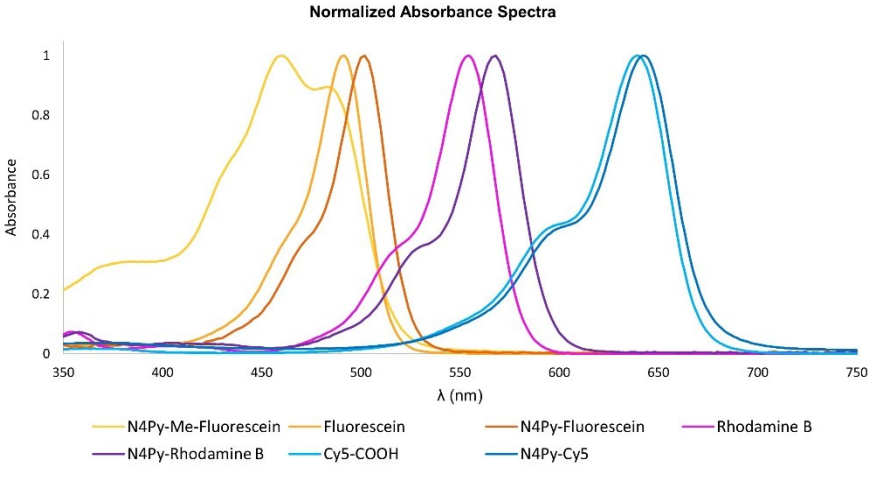

Figure S1. Normalized UV-Vis absorbance spectra of N4Py-conjugates and parent fluorophores in PBS buffer (pH 7.4, 37°C).

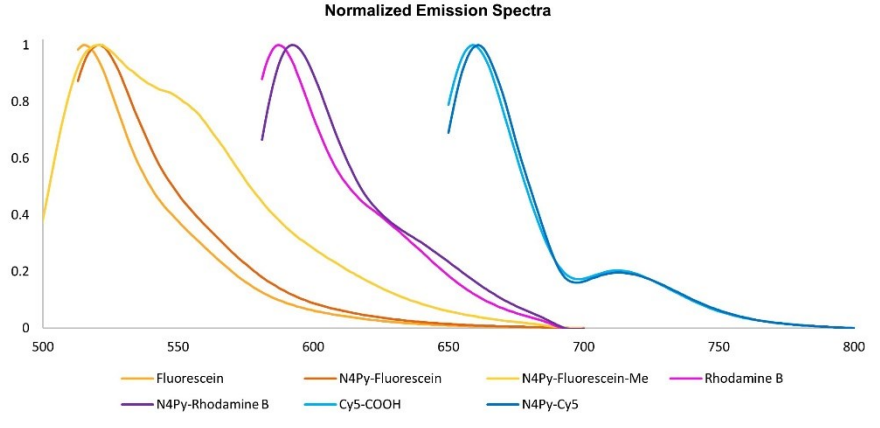

Figure S2. Normalized emission spectra of N4Py-fluorophores and parent fluorophores in PBS buffer (pH 7.4, 37°C).

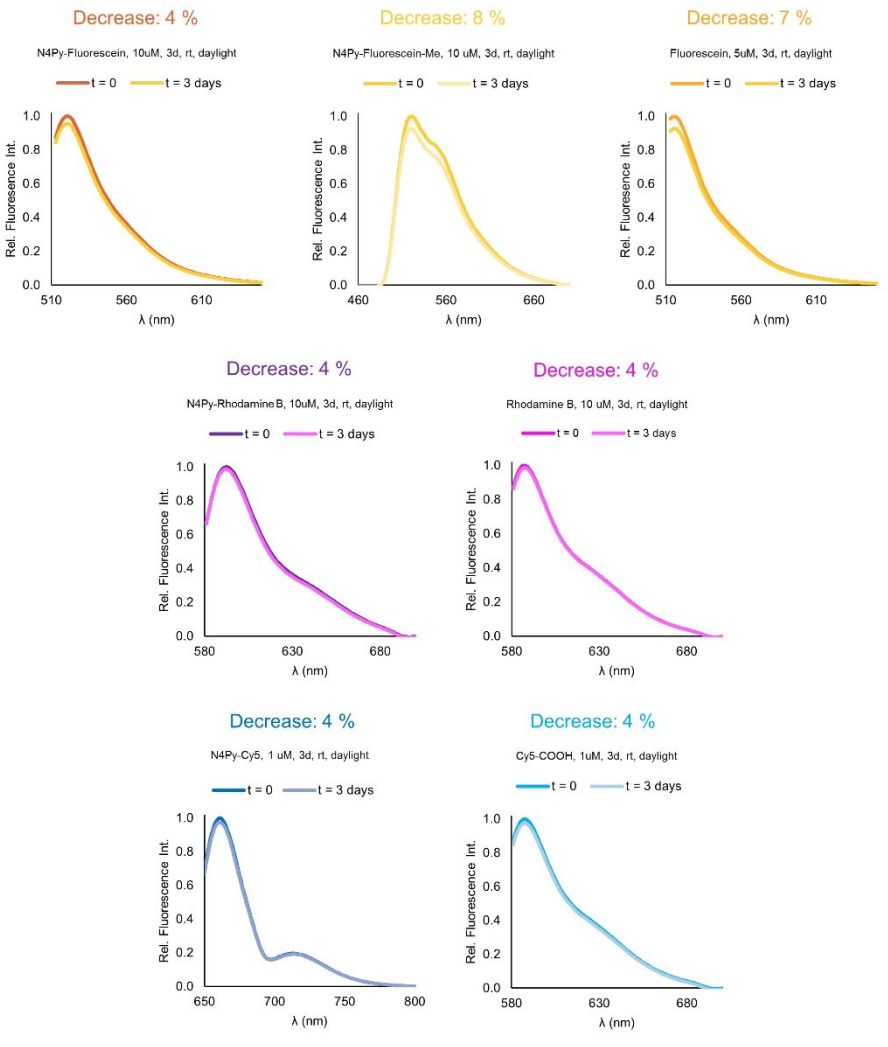

Figure S3. Relative fluorescence intensities for N4Py-conjugates after 3 days at ambient conditions in PBS buffer, pH 7.4.

Photostability studies were performed with concentrations of the fluorophores for which the absorbance did not exceed A_{max} = 0.15 (generally 1-10 µM) in PBS buffer at pH 7.4 (in order to mimic physiological conditions). Compounds were continuously irradiated in the spectrofluorimeter at the indicated maximum excitation wavelength of the fluorophore and spectra were recorded at t = 0, 1, 2, 3, 4, 10, 15, 30, 45, 60 min. The indicated decay (%) is taken over the total of 60 min.

The stability of the fluorophores over a period of 3 days was tested by recording a

spectrum at t = 0 days and t = 3 days, during which the samples were left in broad daylight on a lab bench at room temperature in PSB buffer pH 7.4 (in order to mimic physiological conditions). The indicated decay is taken over the total period of 3 days (%).

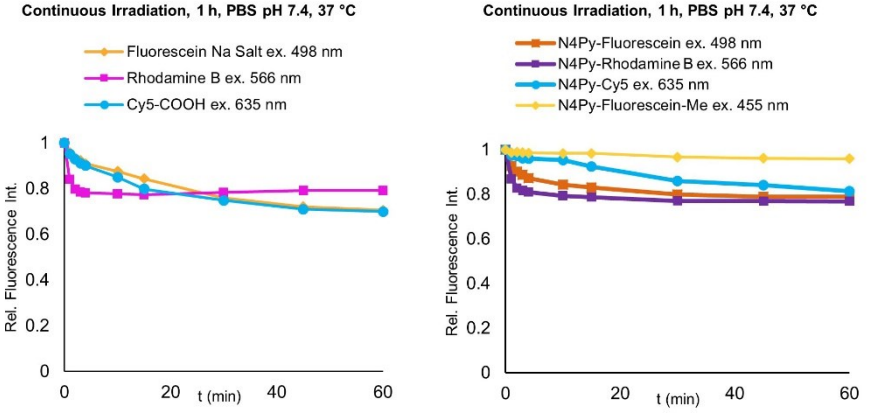

Figure S4. Relative fluorescence intensities for N4Py-conjugates during a 1 h irradiation at excitation wavelength in PBS buffer, pH 7.4 at 37°C.

3.5.4 DNA Cleavage Experiments

3.5.4.1 Materials, Instrumentation and Plasmid Isolation

pUC18 plasmid DNA was isolated from *Escherichia coli* XL1 Blue and purified using a QIAGEN maxi kit. Concentrations were determined by UV-Vis spectrometry at 260 nm using a NanoDrop 1000 spectrophotometer (Thermo Fisher Scientific). DNA ladder (SmartLadder 200-10000 bp) was purchased from Eurogentec. Agarose for gel electrophoresis was purchased from Sigma-Aldrich (bioreagent grade). Ethidium bromide (10 mg/mL in water, bioreagent) was purchased from Sigma-Aldrich. DNA gel loading dye (6x concentrated) was purchased from Thermo Fisher Scientific. Pictures from the agarose gels were taken with a UVIdoc HD2 camera system from UVITEC Cambridge. Quantification of the agarose gel bands was performed using GelQuant.NET software provided by biochemlabsolutions.com. Statistical calculations were performed using Mathematica version 9.0.0.0.

3.5.4.2 DNA Cleavage Experiments

Stock solutions (10 mM) of N4Py and N4Py conjugates were made in pure DMSO (BioReagent, Sigma-Aldrich) and diluted with Milli Q water to a final working concentration of 1 µM. 1 equiv. of $(NH_4)_2Fe(II)(SO_4)_2 \cdot 6H_2O$ was added to the N4Py

ligands in water to form the Fe(II)-complexes *in situ*. The respective solutions of Fe(II)-complexes were added to a buffered solution (Tris-HCl, 10 mM, pH 8.0) in the presence of supercoiled pUC18 plasmid DNA and dithiolthreitol (DTT) in 1.5 mL Eppendorf tubes incubated at 37 °C. The final reaction volume of 50 µL contained a final concentration of 1.0 µM Fe(II)-complex, 0.1 µg/µL DNA and 1.0 mM DTT.

Samples (2 µL) were taken from the reaction solutions at t = 0, 1, 2.5, 5, 7.5, 10, 15, 20, 30, 40, 50, 60 min and were directly quenched in a 18 µL quenching solution, containing 15 µL NaCN solution (1 mg/mL) and 3 µL loading buffer (consisting of 0.03 % bromophenol blue, 0.03 % xylene cyanol FF, 60 % glycerol, 60 mM EDTA, 6x concentrated), after which each sample was directly frozen in liquid nitrogen. The samples were run on 1.2 % agarose gels in TAE buffer for 90 minutes at 70 V. Gels were post stained in an ethidium bromide bath (1.0 µg/mL) for 45 min and washed with TAE buffer. Pictures of the agarose gels were taken for quantification purposes and a correction factor of 1.31 was used for reduced uptake efficiency of ethidium bromide in supercoiled plasmid pUC18 DNA.[51] Results were obtained from experiments that were performed at least in triplicate.

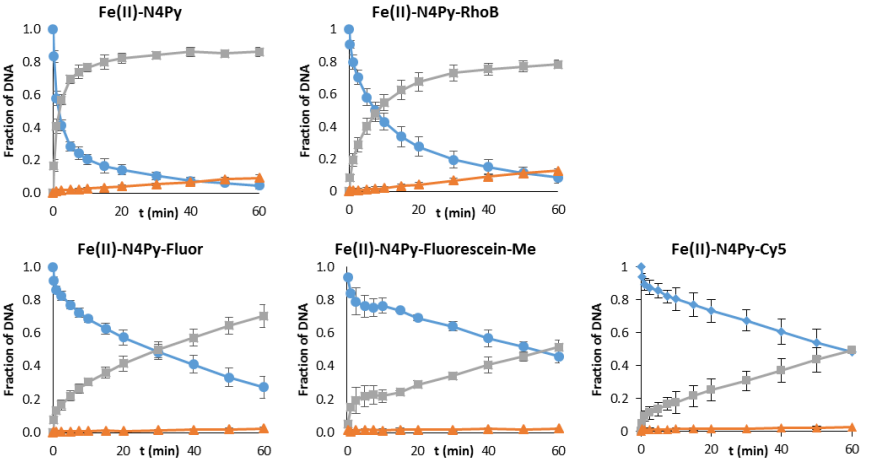

Figure S5. DNA cleavage by iron complexes of N4Py-conjugates. Cleavage of supercoiled DNA (form I, ●) to give nicked (form II, ■) and linear DNA (form III, ▲). Time profile for cleavage with: (top, from left to right) Fe(II)-N4Py, Fe(II)-N4Py-Rhodamine B, (bottom, from left to right) Fe(II)-N4Py-Fluorescein, Fe(II)-N4Py-Fluorescein-Me, Fe(II)-N4Py-Cy5. Conditions: Tris-HCl buffer (pH 8.0) at 37°C, 1.0 µM complex, 0.1 µg/µL pUC18 plasmid DNA (150 µM in base pairs), 1.0 mM DTT. Error bars represent the root mean square based on at least three runs. A correction factor was used to compensate for the reduced ethidium bromide uptake capacity of supercoiled DNA.

3.5.4.3 Calculation of Amounts of Single Strand Cuts (*ssc*) and Double Strand Cuts (*dsc*)

The average number of single- (n) and double-strand cuts (m) of a DNA molecule were calculated with Eqn. (1) and (2), in which f_{III} and f_I are the fractions of linear DNA and supercoiled DNA, respectively.[107] Eqn. (3) describes the Freifelder-Trumbo relationship,[57] in which *h* is the maximum distance in base pairs between nicks of opposite strands to generate a double strand cut (*i.e.* 16), *L* is the total number of base pairs of the DNA molecule used (2686 bp for pUC18 plasmid DNA). Uncertainty values for *m* and *n* were calculated by a Monte-Carlo simulation as described previously.[51,52]

(1) $$f_{III} = m \cdot e^{-m}$$

(2) $$f_I = e^{-(m+n)}$$

(3) $$m = \frac{n^2(2h+1)}{4L}$$

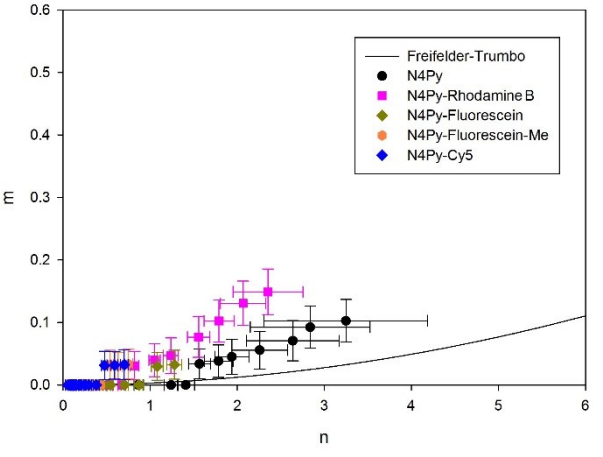

Figure S6. Quantification of the number of double-strand cuts (*m*) as a function of single-strand cuts (*n*) per DNA molecule for each of the N4Py-conjugates. Error bars represent the uncertainty limits of *n* and *m*, based on Monte-Carlo simulations, taking into account a standard deviation σ of 0.03 for each individual data point. The solid black line describes a pure single strand cleavage pathway, as described by the Freifelder-Trumbo relationship.

3.5.4.4 Calculation of Cleavage Rates

The average number of single strand cuts per DNA molecule for a single strand DNA cutting agent can be calculated using Eqn. 4 (when no linear DNA is observed) or Eqn. 5 (when linear DNA is observed).[108,109] Uncertainty values for *n* were calculated

by a Monte-Carlo simulation. The rate constant (k_{obs}) of single-strand DNA cleavage can be determined from the linear fit of the calculated values of *n* as a function of time. In order to take into account the [DNA] (0.1 µg/µL) and [Fe(II)-complexes] (1.0 µM), k_{obs} is corrected into k^* by Eqn. 6.

(4) $f_I = e^{-n}$

(5) $f_I + f_{II} = [1 - n(2h + 1)/2L]^{n/2}$

(6) $k^* = k_{obs} \cdot \frac{[DNA]}{[complex]}$

3.5.5 Cell Experiments

3.5.5.1 Cell Culture

SKOV3 cells (human ovarian carcinoma) were obtained from the ATCC (Manassas, VA). Cells were cultured in Dulbecco's modified Eagle's medium (DMEM) (Lonza, Verviers, Belgium) supplemented with 10% FCS (Perbio Hyclone, Etten-Leur, The Netherlands), 50 µg/mL gentamycine sulfate (Invitrogen, Breda, The Netherlands), 2 mM L-glutamine (Lonza) and incubated at 37°C in a humidified 5% CO_2 incubator.

3.5.5.2 *In Vitro* Cytotoxicity

The viability of cells in the presence and absence of reagents was determined by the MTS assay, as described previously.[53] In short, 6400 cells were seeded in 96-well plates. The following day cells were treated with the fluorophore conjugated N4Py molecules, or 0.1% DMSO as a control. After 24 h, 20 µL of CellTiter 96 Aqueous One Solution (Promega, Madison, WI) was added and incubated for 3 h. The absorbance at 490 nm was measured using a Varioskan plate reader (Thermo Electron Corp., Breda, the Netherlands) and subtracted with the absorbance of cell-free medium containing reagents. For each experiment, every treatment was performed three times, and the experiment was carried out in triplo.

3.5.5.3 Cell Death Analysis

Cells were treated with the fluorophore conjugated N4Py ligands with or without 20 µM of the pan-caspase inhibitor zVAD-FMK. 24h after treatment, both floating and adherent cells were harvested and stained with 5 µg/mL PI (Sigma-Aldrich)/PBS. After a 10 min incubation at 4°C in the dark, fluorescence was measured using the FL-2 (Cy5) or FL-3 (Fluorescein, Rhodamine B) channel of a FACScalibur flow cytometer (Beckton Dickenson Biosciences, San Jose, CA). Background fluorescence was determined by measuring the N4Py-fluorophores alone.

Experiments were conducted in triplicate. The percentage PI positive cells was determined with Kaluza 1.2 (Beckman Coulter) software.

3.5.5.4 dsDNA Breaks

The induction of dsDNA damage in the healthy/early apoptotic population (subG1 population) was determined using FACS analysis of intracellular γH2AX as described before.[53] After 24h treatment with N4Py-fluorophores, cells were fixed in 4% formaldehyde for 10 min at 37 °C and permeabilized in 90% methanol for 30 min on ice. Cells were stained for 30 minutes at RT with a 1:50 dilution of phospho-histone H2A.X (γH2AX) (ser139) (20E3) antibody conjugated to Alexa fluor 488 or 647 (Cell Signaling, Leiden, The Netherlands), for the N4Py-Cy5 or N4Py-Rhodamine B conjugate respectively. After γH2AX staining, cells were washed with PBS and stained with 5 µg/mL PI. After a 10 min incubation at 4°C in the dark, PI fluorescence was determined in the FL2 channel, and γH2AX fluorescence was determined in the FL1 (Alexa 488 conjugate) or FL4 channel (Alexa 647 conjugate) of a FACScalibur flow cytometer. Cells in the subG1 population were excluded from analysis of dsDNA breaks in early/non-apoptotic cells. The cutoff for a γH2AX positive cell was set based on a level of ∼5% positivity in the solvent control. Each experiment was carried out three times. MFI and PI low cells were determined with Kaluza 1.2 (Beckman Coulter) software.

3.5.5.5 ROS Detection

After 24 h treatment with the different N4Py variants, cells were treated with either 5 µM APF (Molecular Probes) and 100 µM H_2O_2 or 5 µM MitoSOX Red (Molecular Probes) for 30 min at 37^0C. After loading the cells with the ROS probe, cells were washed with PBS and collected. For the detection of secondary ROS, APF signal was detected in the FL1 channel of a flow cytometer (BD FACSCalibur, BD Biosciences). For the detection of mitochondrial $O_2^{\bullet-}$, the Mitosox Red signal was detected by flow cytometry (BD LSR-II, BD Biosciences) using a 355 nm UV-laser in combination with a 575/26 nm filter.[71]

3.5.5.6 Confocal Microscopy

Temperature-dependent cellular influx of the N4Py conjugates, N4Py and Fe(II)-N4Py was determined during a 24 h treatment at different temperatures (4 °C, 25.8 °C, 37°C). Necrotic/late apoptotic cells were stained using PI (10 min. incubation, 5 µg/mL PI). Localization and cytotoxicity were visualized using confocal fluorescent microscopy (Leica SP8, HC PL APO CS 10x/0.30 lens, HC PL APO CS2 40x/1,3).

Colocalization of the N4Py conjugates with lysosomes or mitochondria was visualized using confocal fluorescent microscopy (Leica SP8, HC PL APO CS2 63x/1.4 lens). Lysosomes were stained by treating cells with 1x Lysobrite Red solution (AAT Bioquest), 50 nM Lysotracker Green (Molecular Probes) or 100 nM Lysotracker Deep Red (Molecular Probes) for 1h at 37 °C. Mitochondria were stained by treating cells with 200 nM Mitotracker Green (Molecular Probes) or 100 nM Mitotracker Deep Red FM (Molecular Probes) for 30 min at 37 °C. Lysotracker Green, Mitotracker Green and N4Py-Fluorescein were excited using a 488 nm laser light, Lysobrite Red and N4Py-Rhodamine were excited using a 552 nm laser light and Mitotracker Deep Red, Lysotracker Deep Red and N4Py-Cy5 were excited using a 633 nm laser light.

Colocalization studies were performed according to the guidelines of K. W. Dunn *et al.*[110] Images were first analyzed with Leica Application Suite AF Lite software v. 3.2.0.9652 from Leica microsystems and subsequently loaded into ImageJ v. 1.50f as 8-bit black & white images with a 2048x2048 resolution. Whenever possible, signal saturation was avoided and saturated pixels were omitted from quantification. Colocalization Finder plugin for ImageJ v.1.2 (C. Laummonerie, J. Mutterer, Institute de Biologie Moleculaire des Plantes, Strasbourg, France) was used to obtain a composite and mask image and cytofluorogram scatterplot. Colocalization was quantified using Pearson's Correlation Coefficient (PCC)[65] for at least 12 independent Regions Of Interest (ROI) using Coloc 2 plugin (D. J. White, T. Kazimiers, J. Schindelin) from Fiji ImageJ plugin package.[111] Statistical significance of colocalization was analyzed for entire pictures with JACoP plugin v.2.1.1 for ImageJ[112] using Costes's randomization method[113] with xy blocksize of 20 pixels and 1000 randomization rounds. Statistical significance with ROIs was analyzed similarly in Coloc 2.

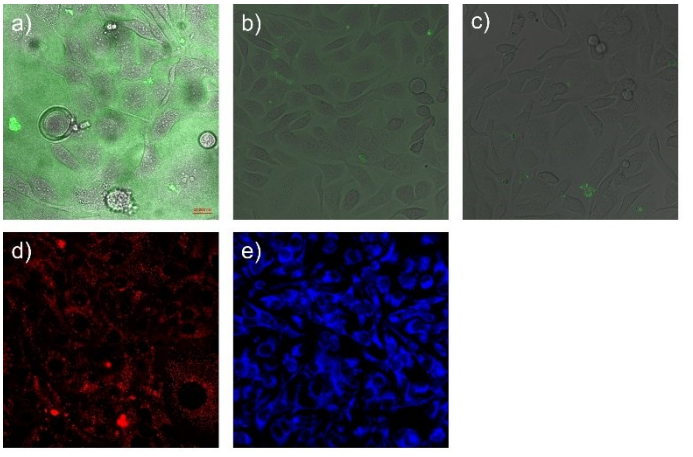

Figure S7. Localization of N4Py-conjugates. SKOV3 cells were treated for 24 h with 10 µM (**a**) N4Py-Fluorescein, (**b**, **c**) N4Py-Me-Fluorescein, (**d**) N4Py-Rhodamine B or (**e**) N4Py-Cy5. Confocal images were taken before (**a**, **b**) or after (**c**, **d**, **e**) washing the cells with PBS. After washing the cells with PBS, all emission was lost for the N4Py-Fluorescein conjugates (only N4Py-Me-Fluorescein data shown in **c**).

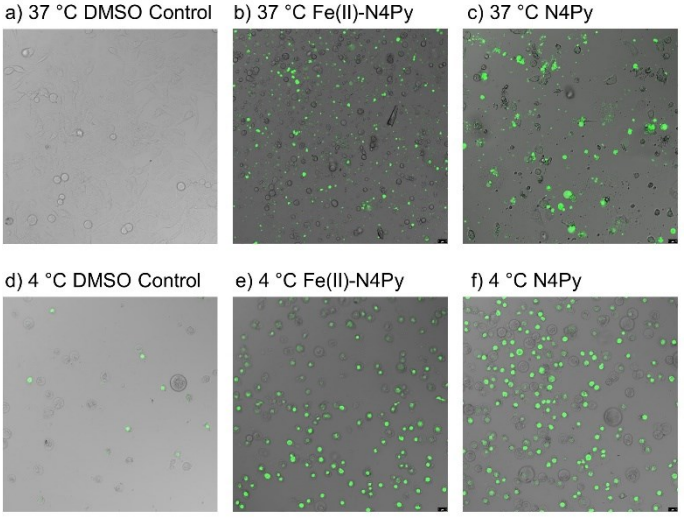

Figure S8. The effect of temperature (T = 37 °C and 4 °C) on the parental N4Py molecule. SKOV3 cells were treated for 24 h at 37 °C (**a-c**) or 4 °C (**d-f**) with 0.1 % DMSO (**a**, **d**), 30 µM Fe(II)-N4Py (**b**, **e**) or 30 µM N4Py ligand (**c**, **f**). Necrotic/late apoptotic cells were stained with propidium iodide (green fluorescence).

3.5.5.7 DNA Isolation

Cell were lysed O/N at 55 °C in TNE lysis buffer (10 mM Tris/HCl, pH 7.5; 150 mM NaCl; 10 mM EDTA; 1% SDS) supplemented with 100 µg proteinase K. Total cellular DNA (genomic and mitochondrial DNA) was extracted using chloroform/isoamyl alcohol (24 : 1), including a 1 h RNase A (Thermo Scientific) treatment at 37 °C, and precipitated using isopropanol.

3.5.5.8 Mitochondrial DNA (mtDNA) Copy Number

10 ng of total cellular DNA was used as input of the qPCR. Primers amplifying a single-copy nDNA region (β-actin) and an mtDNA region (D-loop) were used (Table S2). The mtDNA copy number was calculated with Eqn. 7.

(7) $2^{(\text{Ct nDNA} * \text{primer efficiency} - \text{Ct mtDNA} * \text{primer efficiency})}$

Table S2. Primer sequences

Target		Fw primer sequence (5'-3')	Rv primer sequence (5'-3')
mtDNA ratio	D-loop	TCACCCTATTAACCACTCACGG	ATACTGCGACATAGGGTGCTC
nDNA ratio	β-actin	TGAGTGGCCCGCTACCTCTT	CGGCAGAAGAGAGAACCAGTGA

3.5.5.9 Statistics

All data are presented as the mean ± SEM and were evaluated by a one-way ANOVA followed by Dunnett's post-hoc test. Data was considered statistically significant with a p value < 0.05.

3.6 References

(1) Umezawa, H.; Maeda, K.; Takeuchi, T.; Okami, Y. *J. Antibiot.* **1966**, *19* (5), 200.

(2) Umezawa, H.; Suhara, Y.; Takita, T.; Maeda, K. *J. Antibiot.* **1966**, *19* (5), 210.

(3) Stubbe, J.; Kozarich, J. W. *Chem. Rev.* **1987**, *87* (5), 1107.

(4) Kane, S. A.; Hecht, S. M. *Prog. Nucleic Acid Res. Mol. Biol.* **1994**, *49*, 313.

(5) Claussen, C. A.; Long, E. C. *Chem. Rev.* **1999**, *99* (9), 2797.

(6) Hecht, S. M. *J. Nat. Prod.* **2000**, *63* (1), 158.

(7) Chen, J.; Stubbe, J. *Nat. Rev. Cancer* **2005**, *5* (2), 102.

(8) Costas, M.; Mehn, M. P.; Jensen, M. P.; Que Jr., L. *Chem. Rev.* **2004**, *104* (2),

939.

(9) Guajardo, R. J.; Hudson, S. E.; Brown, S. J.; Mascharak, P. K. *J. Am. Chem. Soc.* **1993**, *115* (18), 7971.

(10) Guajardo, R. J.; Chavez, F.; Farinas, E. T.; Mascharak, P. K. *J. Am. Chem. Soc.* **1995**, *117* (13), 3883.

(11) Kittaka, A.; Sugano, Y.; Otsuka, M.; Ohno, M.; Sugiura, Y.; Umezawa, H. *Tetrahedron Lett.* **1986**, *27* (31), 3631.

(12) Otsuka, M.; Kittaka, A.; Ohno, M.; Suzuki, T.; Kuwahara, J.; Sugiura, Y.; Umezawa, H. *Tetrahedron Lett.* **1986**, *27* (31), 3639.

(13) Kimura, E.; Kurosaki, H.; Kurogi, Y.; Shionoya, M.; Shiro, M. *Inorg. Chem.* **1992**, *31* (21), 4314.

(14) Kurosaki, H.; Hayashi, K.; Ishikawa, Y.; et al. *Inorg. Chem.* **1999**, *38* (12), 2824.

(15) Bernal, I.; Jensen, I. M.; Jensen, K. B.; et al. *J. Chem. Soc., Dalton Trans.* **1995**, *94* (22), 3667.

(16) Mialane, P.; Nivorojkine, A.; Pratviel, G.; et al. *Inorg. Chem.* **1999**, *38* (6), 1085.

(17) Goto, M.; Ishikawa, Y.; Ishihara, T.; et al. *Chem. Commun.* **1997**, *115* (6), 539.

(18) Ishikawa, Y.; Morishita, Y.; Yamamoto, T.; Kurosaki, H.; Goto, M.; Matsuo, H.; Sugiyama, M. *Chem. Lett.* **1998**, *27* (1), 39.

(19) Kurosaki, H.; Maruyama, A.; Koike, H.; Kuroda, N.; Ishikawa, Y.; Goto, M. *Bioorg. Med. Chem. Lett.* **2002**, *12* (2), 201.

(20) Mukherjee, A.; Dhar, S.; Nethaji, M.; et al. *Dalton Trans.* **2005**, *11* (2), 349.

(21) Kurosaki, H.; Ishikawa, Y.; Hayashi, K.; et al. *Inorg. Chim. Acta* **1999**, *294* (1), 56.

(22) Hemmert, C.; Pitié, M.; Renz, M.; Gornitzka, H.; Soulet, S.; Meunier, B. *J. Biol. Inorg. Chem.* **2001**, *6* (1), 14.

(23) Wong, E. L.-M.; Fang, G.-S.; Che, C.-M.; et al. *Chem. Commun.* **2005**, *369* (36), 4578.

(24) Kwong, W.-L. L.; Lok, C.-N. N.; Tse, C.-W. W.; Wong, E. L.-M. ai M.; Che, C.-M. M. *Chem. - Eur. J.* **2015**, *21* (7), 3062.

(25) Chen, J.; Luo, Z.; Zhao, Z.; Xie, L.; Zheng, W.; Chen, T. *Biomaterials* **2015**, *71*, 168.

(26) Abosede, O. O.; Vyas, N. A.; Singh, S. B.; et al. *Dalton Trans.* **2016**, *45* (7), 3003.

(27) Zhou, X.-Q. Q.; Sun, Q.; Jiang, L.; et al. *Dalton Trans* **2015**, *44* (20), 9516.

(28) Zhou, W.; Wang, X.; Hu, M.; et al. *Chem. Sci.* **2014**, *5* (7), 2761.

(29) Soler, M.; Figueras, E.; Serrano-Plana, J.; et al. *Inorg. Chem.* **2015**, *54* (22), 10542.

(30) Bortolotto, T.; Silva-Caldeira, P. P.; Pich, C. T.; Pereira-Maia, E. C.; Terenzi, H. *Chem. Commun* **2016**, *7130* (52), 7130.

(31) Silva, P. P.; Guerra, W.; Dos Santos, G. C.; et al. *J. Inorg. Biochem.* **2014**, *132* (1), 67.

(32) Seng, H.-L. L.; Wang, W.-S. S.; Kong, S.-M. M.; et al. *BioMetals* **2012**, *25* (5), 1061.

(33) Salimi, M.; Abdi, K.; Kandelous, H. M.; Hadadzadeh, H.; Azadmanesh, K.; Amanzadeh, A.; Sanati, H. *BioMetals* **2015**, *28* (2), 267.

(34) Nagababu, P.; Barui, A. K.; Thulasiram, B.; Devi, C. S.; Satyanarayana, S.; Patra, C. R.; Sreedhar, B. *J. Med. Chem.* **2015**, *58* (13), 5226.

(35) Han, T. Y.; Guan, T. S.; Iqbal, M. A.; Haque, R. a.; Sharmila Rajeswari, K.; Khadeer Ahamed, M. B.; Abdul Majid, A. M. S. *Med. Chem. Res.* **2014**, *23* (5), 2347.

(36) Jany, T.; Moreth, A.; Gruschka, C.; et al. *Inorg. Chem.* **2015**, *54* (6), 2679.

(37) Suntharalingam, K.; Hunt, D. J.; Duarte, A. A.; White, A. J. P.; Mann, D. J.; Vilar, R. *Chem. - Eur. J.* **2012**, *18* (47), 15133.

(38) Gao, C.-Y.; Qiao, X.; Ma, Z.-Y.; et al. *Dalton Trans.* **2012**, *41* (39), 12220.

(39) Zhang, Y.-P. P.; Ma, Z.-Y. Y.; Gao, C.-Y. Y.; et al. *New J. Chem.* **2016**, *40* (9), 7513.

(40) Liu, S.; Cao, W.; Yu, L.; et al. *Dalton Trans.* **2013**, *42* (16), 5932.

(41) Cooper, G. M. *The Cell: A Molecular Approach, Tools of Cell Biology*, 2nd ed.; Sinauer Associates, 2000.

(42) Lodish, H.; Berk, A.; Zipursky, S. L.; Matsudaira, P.; Baltimore, D.; Darnell, J. *Molecular Cell Biology: Microscopy and Cell Architecture*, 4th ed.; W. H. Freeman, 2000.

(43) Lubben, M.; Meetsma, A.; Wilkinson, E. C.; Feringa, B.; Que, L. *Angew. Chem. Int. Ed. Engl.* **1995**, *34* (13–14), 1512.

(44) Roelfes, G.; Vrajmasu, V.; Chen, K.; et al. *Inorg. Chem.* **2003**, *42* (8), 2639.

(45) Roelfes, G.; Lubben, M.; Chen, K.; et al. *Inorg. Chem.* **1999**, *38* (8), 1929.

(46) Ho Y. N., R.; Que Jr., L.; Roelfes, G.; Feringa, B. L.; Hermant, R.; Hage, R. *Chem. Commun.* **1999**, No. 21, 2161.

(47) Roelfes, G.; Lubben, M.; Leppard, S. W.; et al. *J. Mol. Cat. A Chem.* **1997**, *117* (1–3), 223.

(48) Ho, R. Y. N.; Roelfes, G.; Feringa, B. L.; Que, L.; Uni, V.; Tpa, L. *J. Am. Chem. Soc.* **1999**, *121* (1), 264.

(49) Roelfes, G.; Branum, M. E.; Wang, L.; Que Lawrence; Feringa, B. L. *J. Am. Chem. Soc.* **2000**, *122* (46), 11517.

(50) Li, Q.; van den Berg, T. A.; Feringa, B. L.; Roelfes, G. *Dalton Trans.* **2010**, *39* (34), 8012.

(51) van den Berg, T. A.; Feringa, B. L.; Roelfes, G. *Chem. Commun.* **2007**, 180.
(52) Megens, R. P.; van den Berg, T. A.; de Bruijn, A. D.; Feringa, B. L.; Roelfes, G. *Chem. - Eur. J.* **2009**, *15* (7), 1723.
(53) Li, Q.; van der Wijst, M. G.; Kazemier, H. G.; Rots, M. G.; Roelfes, G. *ACS Chem. Biol.* **2014**, *9* (4), 1044.
(54) Tounekti, O.; Kenani, A.; Foray, N.; Orlowski, S.; Mir, L. M. *Br. J. Cancer* **2001**, *84* (9), 1272.
(55) Sjöback, R.; Nygren, J.; Kubista, M. *Spectrochim. Acta Part A Mol. Biomol. Spectrosc.* **1995**, *51* (6), L7.
(56) Sjöback, R.; Nygren, J.; Kubista, M. *Biopolymers* **1998**, *46* (7), 445.
(57) Freifelder, D.; Trumbo, B. *Biopolymers* **1969**, *7* (5), 681.
(58) Wlodkowic, D.; Skommer, J.; Darzynkiewicz, Z. *Methods Mol. Biol.* **2009**, *559*, 19.
(59) Darzynkiewicz, Z.; Juan, G.; Li, X.; Gorczyca, W.; Murakami, T.; Traganos, F. *Cytometry* **1997**, *27* (1), 1.
(60) Olive, P. L. *Methods Cell Biol.* **2004**, *75*, 355.
(61) Davies, C. W.; Chaney, J.; Korbel, G.; Ringe, D.; Petsko, G. A.; Ploegh, H.; Das, C. *Bioorg. Med. Chem. Lett.* **2012**, *22* (12), 3900.
(62) Roelfes, G.; Lubben, M.; Hage, R.; Que Jr, L.; Feringa, B. L. *Chem. - Eur. J.* **2000**, *6* (12), 2152.
(63) Setsukinai, K. ichi; Urano, Y.; Kakinuma, K.; Majima, H. J.; Nagano, T. *J. Biol. Chem.* **2003**, *278* (5), 3170.
(64) Gao, J.; Wang, P.; Giese, R. W. *Anal. Chem.* **2002**, *74* (24), 6397.
(65) Manders, E. M.; Stap, J.; Brakenhoff, G. J.; van Driel, R.; Aten, J. A. *J. Cell Sci.* **1992**, *103* (3), 857.
(66) Komai, T.; Shigehara, E.; Tokui, T.; Koga, T.; Ishigami, M.; Kuroiwa, C.; Horiuchi, S. *Biochem. Pharmacol.* **1992**, *43* (4), 667.
(67) Lancon, A.; Delmas, D.; Osman, H.; Thenot, J. P.; Jannin, B.; Latruffe, N. *Biochem. Biophys. Res. Commun.* **2004**, *316* (4), 1132.
(68) Ufuk, A.; Somers, G.; Houston, J. B.; Galetin, A. *Pharm. Res.* **2015**, *32* (12), 3937.
(69) Shokolenko, I.; Venediktova, N.; Bochkareva, A.; Wilson, G. L.; Alexeyev, M. F. *Nucleic Acids Res.* **2009**, *37* (8), 2539.
(70) Murphy, M. P. *Biochem. J.* **2009**, *417* (1), 1.
(71) Robinson, K. M.; Janes, M. S.; Beckman, J. S. *Nat. Protoc.* **2008**, *3* (6), 941.
(72) Robinson, K. M.; Janes, M. S.; Pehar, M.; et al. *Proc. Natl. Acad. Sci.* **2006**, *103* (41), 15038.
(73) Zielonka, J.; Srinivasan, S.; Hardy, M.; et al. *Free Rad. Biol. Med.* **2008**, *44* (5), 835.

(74) Wallace, D. C. *Annu. Rev. Genet.* **2005**, *39*, 359.
(75) Ding, W. X.; Yin, X. M. *Biol. Chem.* **2012**, *393* (7), 547.
(76) Lee, J.; Giordano, S.; Zhang, J. *Biochem. J.* **2012**, *441* (2), 523.
(77) Chikte, S.; Panchal, N.; Warnes, G. *Cytom. A J. Int. Soc. Anal. Cytol.* **2014**, *85* (2), 169.
(78) Bröker, L. E.; Kruyt, F. A. E.; Giaccone, G. *Clin. Cancer Res.* **2005**, *11* (9), 3155.
(79) Vanden Berghe, T.; Linkermann, A.; Jouan-Lanhouet, S.; Walczak, H.; Vandenabeele, P. *Nat. Rev. Mol. Cell Biol.* **2014**, *15* (2), 135.
(80) Moubarak, R. S.; Yuste, V. J.; Artus, C.; Bouharrour, A.; Greer, P. A.; Menissier-de Murcia, J.; Susin, S. A. *Mol. Cell. Biol.* **2007**, *27* (13), 4844.
(81) Artus, C.; Boujrad, H.; Bouharrour, A.; et al. *EMBO J.* **2010**, *29* (9), 1585.
(82) van Wijk, S. J.; Hageman, G. J. *Free Rad. Biol. Med.* **2005**, *39* (1), 81.
(83) Igney, F. H.; Krammer, P. H. *Nat. Rev.* **2002**, *2* (4), 277.
(84) Wolf, B. B.; Schuler, M.; Li, W.; et al. *J. Biol. Chem.* **2001**, *276* (36), 34244.
(85) Lavis, L. D.; Rutkoski, T. J.; Raines, R. T. *Anal. Chem.* **2007**, *79* (17), 6775.
(86) Sun, W.-C.; Gee, K. R.; Klaubert, D. H.; Haugland, R. P. *J. Org. Chem.* **1997**, *62* (19), 6469.
(87) Guilbault, G. G.; Kramer, D. N. *Anal. Chem.* **1964**, *36* (2), 409.
(88) Boyd, V.; Cholewa, O. M.; Papas, K. K. *Curr. Trends Biotechnol. Pharm.* **2008**, *2* (2), 66.
(89) Reungpatthanaphong, P.; Dechsupa, S.; Meesungnoen, J.; Loetchutinat, C.; Mankhetkorn, S. *J. Biochem. Biophys. Methods* **2003**, *57* (1), 1.
(90) Luzio, J. P.; Pryor, P. R.; Bright, N. A. *Nat. Rev. Mol. Cell Biol.* **2007**, *8* (8), 622.
(91) Ciechanover, A. *Cell Death Differ.* **2005**, *12* (9), 1178.
(92) Alford, R.; Simpson, H. M.; Duberman, J.; et al. *Mol. Imaging* **2009**, *8* (6), 341.
(93) Chen, P.; Li, J.; Qian, Z.; Zheng, D.; Okasaki, T.; Hayami, M. *Dye. Pigment.* **1998**, *37* (3), 213.
(94) Oushiki, D.; Kojima, H.; Terai, T.; Arita, M.; Hanaoka, K.; Urano, Y.; Nagano, T. *J. Am. Chem. Soc.* **2010**, *132* (8), 2795.
(95) Toutchkine, A.; Nguyen, D. V; Hahn, K. M. *Org. Lett.* **2007**, *9* (15), 2775.
(96) Lou, Z.; Li, P.; Song, P.; Han, K. *Analyst* **2013**, *138* (21), 6291.
(97) Chen, S.; Galan, M. C.; Coltharp, C.; O'Connor, S. E. *Chem. Biol.* **2006**, *13* (11), 1137.
(98) Walls, T. H.; Grindrod, S. C.; Beraud, D.; et al. *Bioorg. Med. Chem.* **2012**, *20* (17), 5269.
(99) Leriche, G.; Chen, A. C.; Kim, S.; Selkoe, D. J.; Yang, J. *ACS Chem. Neurosci.* **2016**, *7* (1), 40.

(100) Derbre, S.; Roue, G.; Poupon, E.; Susin, S. A.; Hocquemiller, R. *ChemBioChem* **2005**, *6* (6), 979.
(101) Bonnet, D.; Ilien, B.; Galzi, J.-L.; Riche, S.; Antheaune, C.; Hibert, M. *Bioconjug. Chem.* **2006**, *17* (6), 1618.
(102) Yuan, H.; Luo, J.; Field, S.; Weissleder, R.; Cantley, L.; Josephson, L. *Bioconjug. Chem.* **2005**, *16* (3), 669.
(103) Suzuki, K.; Ohtake, A.; Ito, Y.; Kanie, O. *Chem. Commun.* **2012**, *48* (78), 9744.
(104) Huynh, T. H. V; Abrahamsen, B.; Madsen, K. K.; Gonzalez-Franquesa, A.; Jensen, A. A.; Bunch, L. *Bioorg. Med. Chem.* **2012**, *20* (23), 6831.
(105) Sato, S.; Aoyama, H.; Miyachi, H.; Naito, M.; Hashimoto, Y. *Bioorg. Med. Chem. Lett.* **2008**, *18* (11), 3354.
(106) Nguyen, T.; Francis, M. B. *Org. Lett.* **2003**, *5* (18), 3245.
(107) Povirk, L. F.; Wubter, W.; Kohnlein, W.; Hutchinson, F. *Nucleic Acids Res.* **1977**, *4* (10), 3573.
(108) Hertzberg, R. P.; Dervan, P. B. *Biochemistry* **1984**, *23* (17), 3934.
(109) Hertzberg, R. P.; Dervan, P. B. *J. Am. Chem. Soc.* **1982**, *104* (1), 313.
(110) Dunn, K. W.; Kamocka, M. M.; McDonald, J. H. *Am. J. Physiol. Physiol.* **2011**, *300* (4), C723.
(111) Schindelin, J.; Arganda-Carreras, I.; Frise, E.; et al. *Nat. Methods* **2012**, *9* (7), 676.
(112) Bolte, S.; Cordelieres, F. P. *J. Microsc.* **2006**, *224* (3), 213.
(113) Costes, S. V; Daelemans, D.; Cho, E. H.; Dobbin, Z.; Pavlakis, G.; Lockett, S. *Biophys. J.* **2004**, *86* (6), 3993.